

# Weak precipitation, warm winters and springs impact glaciers of south slopes of Mt. Everest (central Himalaya) in the last two decades (1994-2013)

Franco Salerno<sup>(1,4\*)</sup>, Nicolas Guyennon<sup>(2)</sup>, Sudeep Thakuri<sup>(1,4)</sup>, Gaetano Viviano<sup>(1)</sup>, Emanuele Romano<sup>(2)</sup>, Elisa Vuillermoz<sup>(4)</sup>, Paolo Cristofanelli<sup>(3,4)</sup>, Paolo Stocchi<sup>(3)</sup>, Giacomo Agrillo<sup>(3)</sup>, Yaoming Ma<sup>(5)</sup>, Gianni Tartari<sup>(1,4)</sup>

<sup>(1)</sup> National Research Council, Water Research Institute, Brugherio (IRSA -CNR), Italy

<sup>(2)</sup> National Research Council, Water Research Institute, Roma (IRSA-CNR), Italy

<sup>(3)</sup> National Research Council, Institute of Atmospheric Sciences and Climate (ISAC-CNR) Bologna, Italy

<sup>(4)</sup> Ev-K2-CNR Committee, Via San Bernardino, 145, Bergamo 24126, Italy

<sup>(5)</sup> Institute of Tibetan Plateau Research, Chinese Academy of Science, China

*\*Correspondence to Franco Salerno*

Email: salerno@irsa.cnr.it

Address: IRSA-CNR Via Del Mulino 19. Località Occhiate 20861Brugherio (MB)

Phone: +39 039 21694221

Fax: +39 039 2004692

## Abstract

Studies on recent climate trends from the Himalayan range are limited, and even completely absent at high elevation (> 5000 m a.s.l.). This contribution specifically explores the southern slopes of Mt. Everest (central Himalaya), analyzing the minimum, maximum, and mean temperature and precipitation time series reconstructed from seven stations located between 2660 and 5600 m a.s.l. over the last twenty years (1994-2013). We complete this analysis with data from all the existing ground weather stations located on both sides of the mountain range (Koshi Basin) over the same period. Overall we observe that the main and more significant increase in temperature is concentrated outside of the monsoon period. Above 5000 m a.s.l. minimum temperature ( $+0.072 \pm 0.011 \text{ } ^\circ\text{C y}^{-1}$ ,  $p < 0.001$ ) increased far more than maximum temperature ( $+0.009 \pm 0.012 \text{ } ^\circ\text{C y}^{-1}$ ,  $p > 0.1$ ), while mean temperature increased by  $+0.044 \pm 0.008 \text{ } ^\circ\text{C y}^{-1}$ ,  $p < 0.05$ . Moreover, we note a substantial liquid precipitation weakening ( $-9.3 \pm 1.8 \text{ mm y}^{-1}$ ,  $p < 0.01$  during the monsoon season). The annual rate of decrease in precipitation at higher elevation is similar to the one at lower altitudes on the southern side of the Koshi Basin, but the drier conditions of this remote environment make the fractional loss much more consistent (-47% during the monsoon period). This study contributes to change the perspective on which climatic driver (temperature vs. precipitation) led mainly the glacier responses in the last twenty years. The main implications are the following: 1) the negative mass balances of glaciers observed in this region can be more ascribed to

38 less accumulation due to weaker solid precipitation than to an increase of melting  
39 processes. 2) The melting processes have only been favored during winter and spring  
40 months and close to the glaciers terminus. 3) A decreasing of the probability of snowfall  
41 has significantly interested only the glaciers ablation zones (-10 %,  $p < 0.05$ ), but the  
42 magnitude of this phenomenon is decidedly lower than the observed decrease of  
43 precipitation. 4) The lesser accumulation could be the cause behind the observed lower  
44 glacier flow velocity and the current stagnation condition of tongues, which in turn  
45 could have triggered melting processes under the debris glacier coverage, leading to the  
46 formation of numerous supraglacial and proglacial lakes that have characterized the  
47 region in the last decades. Without demonstrating the causes that could have led to the  
48 climate change pattern observed at high elevation, we conclude by listing the recent  
49 literature on hypotheses that accord with our observations.

50 **Keywords:** temperature lapse rate, precipitation gradient, monsoon weakening,  
51 Sequential Mann-Kendall, expectation maximization algorithm, climate change, glaciers  
52 shrinkage, central Himalaya

## 53 **1 Introduction**

54 The current uncertainties concerning the glacial shrinkage in the Himalayas are  
55 mainly attributed to a lack of measurements, both of the glaciers and of climatic forcing  
56 agents (e.g., Bolch et al., 2012). Recent results underline the need for a fine scale inves-  
57 tigation, especially at high altitude, to better model the hydrological dynamics in this ar-  
58 ea. However, there are few high elevation weather stations in the world where the glaci-  
59 ers are located (Tartari et al., 2009). This can be attributed to the remote location of  
60 glaciers, the rugged terrain, and a complex political situation, all of which make physi-  
61 cal access difficult (Bolch et al., 2012). As a consequence of the remoteness and diffi-  
62 culty in accessing many high elevation sites combined with the complications of operat-  
63 ing automated weather stations (AWSs) at these altitudes, long-term measurements are  
64 challenging (Vuille, 2011). However, nearly all global climate models report increased  
65 sensitivity to warming at high elevations (e.g., Rangwala and Miller, 2012), while ob-  
66 servations are less clear (Pepin and Lundquist, 2008). Moreover, changes in the timing or  
67 amount of precipitation are much more ambiguous and difficult to detect, and there is  
68 no clear evidence of significant changes in total precipitation patterns in most mountain  
69 regions (Vuille, 2011).

70 The need for a fine scale investigation is particularly evident on the south slope of  
71 Mt. Everest (central Southern Himalaya, CH-S) as it is one of the heavily glaciated parts  
72 of the Himalaya (Salerno et al., 2012; Thakuri et al., 2014). Nevertheless, these glaciers  
73 have the potential to build up moraine-dammed lakes storing large quantities of water,  
74 which are susceptible to GLOFs (glacial lake outburst floods) (e.g., Salerno et al., 2012;  
75 Fujita et al., 2013). Gardelle et al. (2011) noted that this region is most characterized by  
76 glacial lakes in the Hindu Kush Karakorum Himalaya. Recently, Thakuri et al. (2014)  
77 noted that the Mt. Everest glaciers experienced an accelerated shrinkage in the last

78 twenty years (1992-2011), as underlined by an upward shift of the Snow Line Altitude  
79 (SLA) with a velocity almost three times greater than the previous period (1962-1992).  
80 Furthermore Bolch et al. (2011) and Nuimura et al. (2012) found a higher mass loss rate  
81 during the last decade (2000–2010). Anyway, to date, there are not continuous  
82 meteorological time series able to clarify the causes of the melting process to which the  
83 glaciers of these slopes are subjected.

84 In this context, since the early 1990s, PYRAMID Observatory Laboratory (5050 m  
85 a.s.l.) was created by the *Ev-K2-CNR Committee* ([www.ev-k2-cnr.org](http://www.ev-k2-cnr.org)). This observatory  
86 is located at the highest elevation at which weather data has ever been collected in the  
87 region and thus represents a valuable dataset with which to investigate the climate  
88 change in CH-S (Tartari et al., 2002; Lami et al., 2010). However, the remoteness and  
89 the harsh conditions of the region over the years have complicated the operations of the  
90 AWSs, obstructing long-term measurements from a unique station.

91 In this paper, we mainly explore the small scale climate variability of the south  
92 slopes of Mt. Everest by analyzing the minimum, maximum, and mean air temperature  
93 (T) and liquid precipitation (Prec) time series reconstructed from seven AWSs located  
94 from 2660 to 5600 m a.s.l. over the last couple of decades (1994-2013). Moreover, we  
95 complete this analysis with all existing weather stations located on both sides of the  
96 Himalayan range (Koshi Basin) for the same period. In general, this study has the  
97 ultimate goal of linking the climate change patterns observed at high elevation with the  
98 glacier responses over the last twenty years, during which a more rapid glacier  
99 shrinkage process occurred in the region of investigation.

## 100 **2 Region of investigation**

101 The current study is focused on the Koshi (KO) Basin which is located in the eastern  
102 part of central Himalaya (CH) (Yao et al., 2012; Thakuri et al., 2014). To explore  
103 possible differences in the surroundings of Mt. Everest, we decided to consider the  
104 north and south parts of CH (with the suffixes -N and -S, respectively) separately (Fig.  
105 1a). The KO River (58,100 km<sup>2</sup> of the basin) originates in the Tibetan Plateau (TP) and  
106 the Nepali highlands. The area considered in this study is within the latitudes of 27° and  
107 28.5° N and longitudes of 85.5° and 88° E. The altitudinal gradient of this basin is the  
108 highest in the world, ranging from 77 to 8848 m a.s.l., i.e., Mt. Everest. We subdivide  
109 the KO Basin into the northern side (KO-N), belonging to the CH-N, and southern side  
110 (KO-S), belonging to the CH-S. The southern slopes of Mt. Everest are part of the  
111 Sagarmatha (Everest) National Park (SNP) (Fig. 1b), where the small scale climate  
112 variability at high elevation is investigated. The SNP is the world's highest protected  
113 area, with over 30000 tourists in 2008 (Salerno et al., 2010a; Salerno et al., 2013). The  
114 park area (1148 km<sup>2</sup>), extending from an elevation of 2845 to 8848 m a.s.l., covers the  
115 upper Dudh Koshi (DK) Basin (Manfredi et al., 2010; Amatya et al., 2010). Land cover  
116 classification shows that almost one-third of the territory is characterized by glaciers  
117 and ice cover (Salerno et al., 2008; Tartari et al., 2008), while less than 10% of the park  
118 area is forested (Bajracharya et al., 2010; Salerno et al., 2010b). The SNP presents a

119 broad range of bioclimatic conditions with three main bioclimatic zones: the zone of  
120 alpine scrub; the upper alpine zone, which includes the upper limit of vegetation  
121 growth; and the Arctic zone, where no plants can grow (UNEP and WCMC, 2008).  
122 Figure 1c shows the glacier distribution along the hypsometric curve of the SNP. We  
123 observe that the glacier surfaces are distributed from 4300 m to above 8000 m a.s.l.,  
124 with more than 75% of the glacier surfaces lying between 5000 m and 6500 m a.s.l. The  
125 2011 area-weighted mean elevation of the glaciers was 5720 m a.s.l. (Thakuri et al.,  
126 2014). These glaciers are identified as the summer accumulation-type fed mainly by  
127 summer Prec from the South Asian monsoon system, whereas the winter Prec caused by  
128 the mid-latitude westerly wind is minimal (Yao et al., 2012). The prevailing direction of  
129 the monsoons is S-N and SW-NE (e.g., Ichiyanagi et al., 2007). The climate is  
130 influenced by the monsoon system because the area is located in the subtropical zone  
131 with nearly 90% of the annual Prec falling in the months of June to September (this  
132 study). Heavy autumn and winter snowfalls can occur in association with tropical  
133 cyclones and westerly disturbances, respectively, and snow accumulation can occur at  
134 high elevations at all times of the year (Benn, 2012). Bollasina et al. (2002) have  
135 demonstrated the presence of well-defined local circulatory systems in the Khumbu  
136 Valley (SNP). The local circulation is dominated by a system of mountain and valley  
137 breezes. The valley breeze blows (approximately  $4 \text{ m s}^{-1}$ ) from the south every day from  
138 sunrise to sunset throughout the monsoon season, pushing the clouds that bring Prec  
139 northward.

### 140 **3 Data**

#### 141 3.1 Weather stations at high elevation

142 The first automatic weather station (named hereafter AWS0) at 5050 m a.s.l. near  
143 PYRAMID Observatory Laboratory (Fig. 1c), was established in October 1993, it has  
144 run continuously all year round (Bertolani et al., 2000). The station, operating in ex-  
145 treme conditions, had recorded long-term ground-based temperature and temperature  
146 data which are considered valid until December 2005. Due to the obsolescence of tech-  
147 nology, the station was disposed of in 2006. A new station (named hereafter AWS1) was  
148 installed just a few tens of meters away from AWS0 and has been operating since Octo-  
149 ber 2000. Other stations were installed in the following years in the upper DK Basin in  
150 the Khumbu Valley (Table 1). In 2008, the network included sixth monitoring points,  
151 including the highest weather station of the world, located at South Col of Mt. Everest  
152 (7986 m a.s.l.). The locations of all stations are presented in Figure 1b. We can observe  
153 in Figure 1c that this meteorological network represents well the climatic conditions of  
154 the SNP glaciers: AWS0 and AWS1 (5035 m a.s.l.) characterize the glacier fronts (4870  
155 m a.s.l.), AWS4 (5600 m a.s.l.) represents the mean elevation of glaciers in the area  
156 (5720 m a.s.l.), and AWS5, the surface station at South Col (7986 m a.s.l.), characterizes  
157 the highest peaks (8848 m a.s.l.).

158 All stations, except AWS5 (only T), record at least T and Prec. This dataset presents  
159 some gaps (listed in Table 1) as a consequence of the complications of operating AWS  
160 at these altitudes. The list of measured variables for each stations and relevant data can  
161 be downloaded from <http://geonetwork.evk2cnr.org/>. Data processing and quality  
162 checks are performed according to the international standards of the WMO (World Me-  
163 teorological Organization).

164 The Prec sensors at these locations are conventional heated tipping buckets which  
165 may not fully capture the solid Prec. Therefore, solid Prec is probably underestimated,  
166 especially in winter. However, in order to know the magnitude of the possible underes-  
167 timation of the solid phase, we compared the monthly mean Prec of the reconstructed  
168 PYRAMID series (1994-2013 period) with the Prec of a station located downstream at  
169 2619 m a.s.l. (Chaurikhark, ID 1202), (Fig. 1b, Table 2) which presents monthly mean  
170 temperature above 0 °C even during the winter and thus a high prevalence of liquid Prec  
171 also during these months. This comparison, supported by the elevated correlation exist-  
172 ing between the monthly Prec of the two stations, shown a slight underestimation of the  
173 PYRAMID snow (about  $3\pm 1\%$  of total annual precipitation registered at PYRAMID,  
174 see Supplementary material 3 for more details). Therefore, being much reduced the un-  
175 derestimation, we decided not to manipulate data. However the trends hereafter reported  
176 are referred mainly to the liquid phase of Prec. In this regard, according to both Fujita  
177 and Sakai, 2014 and field observations (Ueno et al., 1994), the precipitation phase has  
178 been taken into account assuming that the probability of snowfall and rainfall depends  
179 on mean daily air temperature, using as thresholds – as proposed by the aforementioned  
180 authors – 0 °C and 4 °C, respectively. In Figure 2 we first of all observe that at 5050 m  
181 a.s.l. 90% of precipitation is concentrated during June-September and that the probabilit-  
182 y of snowfall is very low (4%), considering that the mean daily temperature during  
183 these months is above 0 °C. On a yearly basis, this probability reaches 20% of the annu-  
184 al cumulated precipitation.

### 185 3.2 Other weather stations at lower altitude in the Koshi Basin

186 In KO-S Basin (Nepal), the stations are operated by the Department of Hydrology  
187 and Meteorology (DHM) ([www.dhm.gov.np/](http://www.dhm.gov.np/)). For daily T and Prec, we selected 10  
188 stations for T and 19 stations for Prec considering both the length of the series and the  
189 monitoring continuity (< 10% of missing daily data). The selected stations cover an  
190 elevation range between 158 and 2619 m a.s.l. (Table 3). In KO-N Basin (TP, China),  
191 the number of ground weather stations (operated by the Chinese Academy of Science  
192 (CAS)), selected with the same criteria mentioned above, is considerably smaller, just  
193 two, but these stations have a higher elevation (4302 m a.s.l. for the Dingri station and  
194 3811 m a.s.l. for the Nyalam station).

195 The quality insurance of these meteorological data is ensured considering that they  
196 are used as part of global and regional networks including for instance APHRODITE  
197 (Asian Precipitation–Highly Resolved Observational Data Integration Towards

198 Evaluation of Water Resources) (Yasutomi et al., 2011) and GHCN (Global Historical  
199 Climatology Network) (Menne et al., 2012).

## 200 **4 Methods**

201 We define the pre-monsoon, monsoon, and post-monsoon seasons as the months  
202 from February to May, June to September, and October to January, respectively. The  
203 minT, maxT, and meanT are calculated as the minimum, maximum, and mean daily air  
204 temperature. For total precipitation (Prec), we calculate the mean of the cumulative  
205 precipitation for the analyzed period.

### 206 4.1 Reconstruction of the daily temperature and precipitation time series at high 207 elevation

208 The two stations named AWS0 and AWS1 in the last twenty years, considering the  
209 extreme weather conditions of this area, present a percentage of missing daily values of  
210 approximately 20% (Table 1). The other stations (hereafter named secondary stations)  
211 were used here for infilling the gaps according to a priority criteria based on the degree  
212 of correlation among data. AWS1 was chosen as the reference station given the length  
213 of the time series and that it is currently still operating. Therefore, our reconstruction  
214 (hereafter named PYRAMID) is referred to an elevation of 5035 m a.s.l..

215 The selected infilling method is a simple regression analysis based on quantile  
216 mapping (e.g., Déqué, 2007; Themeßl et al., 2012). This regression method has been  
217 preferred to more complex techniques, such as the fuzzy rule-based approach (Abebe et  
218 al., 2000) or the artificial neural networks (Abudu et al., 2010; Coulibaly and Evora,  
219 2007), considering the peculiarity of this case study. In fact, all stations are located in  
220 the same valley (Khumbu Valley). This aspect confines the variance among the stations  
221 to the altitudinal gradient of the considered variable (T or Prec), which can be easily  
222 reproduced by the stochastic link created by the quantile mapping method. In case all  
223 stations registered a simultaneous gap, we apply a multiple imputation technique  
224 (Schneider, 2001) that uses some other proxy variables to fill the remaining missing  
225 data. Details on the reconstruction procedure and the computation of the associated  
226 uncertainty are provided in Supplementary Material 1.

### 227 4.2 The trends analysis: the Sequential Mann-Kendall test

228 The Mann-Kendall (MK) test (Kendall, 1975) is widely adopted to assess significant  
229 trends in hydro-meteorological time series (e.g., Carraro et al., 2012a, 2012b; Guyennon  
230 et al., 2013). This test is non-parametric, thus being less sensitive to extreme sample  
231 values, and is independent of the hypothesis about the nature of the trend, whether  
232 linear or not. The MK test verifies the assumption of the stationarity of the investigated  
233 series by ensuring that the associated normalized Kendall's tau coefficient,  $\mu(\tau)$ , is  
234 included within the confidence interval for a given significance level (for  $\alpha = 5\%$ , the

235  $\mu(\tau)$  is below  $-1.96$  and above  $1.96$ ). In the sequential form (seqMK) (Gerstengarde  
236 and Werner, 1999),  $\mu(\tau)$  is calculated for each element of the sample. The procedure  
237 is applied forward starting from the oldest values (progressive) and backward starting  
238 from the most recent values (retrograde). If no trend is present, the patterns of  
239 progressive and retrograde  $\mu(\tau)$  versus time (i.e., years) present several crossing  
240 points, while a unique crossing period allows the approximate location of the starting  
241 point of the trend (e.g., Bocchiola and Diolaiuti, 2010).

242 In this study, the seqMK is applied to monthly vectors. Monitoring the seasonal non-  
243 stationarity, the monthly progressive  $\mu(\tau)$  is reported with a pseudo color code, where  
244 the warm colors represent the positive slopes and cold colors the negative ones. Color  
245 codes associated with values outside of the range ( $-1.96$  to  $1.96$ ) possess darker tones to  
246 highlight the trend significance (Salerno et al., 2014). Moreover, to monitor the overall  
247 non-stationarity of the time series, both the progressive and the retrograde  $\mu(\tau)$  at the  
248 annual scale are reported. We used the Sen's slope proposed by Sen (1968) as a robust  
249 linear regression allowing the quantification of the potential trends revealed by the  
250 seqMK (e.g., Bocchiola and Diolaiuti, 2010). The significance level is established for  $p$   
251  $< 0.05$ . We define a slight significance for  $p < 0.10$ . The uncertainty associated with the  
252 Sen's slopes (1994-2013) is estimated through a Monte Carlo uncertainty analysis (e.g.,  
253 James and Oldenburg, 1997), described in detail in Supplementary Material 1.

## 254 **5 Results**

### 255 5.1 Trend analysis at high elevation

256 Figure 3 shows the reconstructed PYRAMID time series for minT, maxT, meanT,  
257 and Prec resulting from the overall infilling process explained in Supplementary  
258 Material 1. Figure 4 analyzes the monthly trends of T and Prec from 1994 to 2013 for  
259 PYRAMID.

#### 260 *Minimum air temperature (minT)*

261 November ( $+0.17\text{ }^{\circ}\text{C y}^{-1}$ ,  $p < 0.01$ ) and December ( $+0.21\text{ }^{\circ}\text{C y}^{-1}$ ,  $p < 0.01$ ) present  
262 the highest increasing trend, i.e., both these two months experienced about even  $+4\text{ }^{\circ}\text{C}$   
263 over twenty years (Fig. 4a). In general, the post- and pre-monsoon periods experience  
264 higher and more significant increases than during the monsoon. In particular, we note  
265 the significant and consistent increase of minT of April ( $+0.10\text{ }^{\circ}\text{C y}^{-1}$ ,  $p < 0.05$ ). At the  
266 annual scale, the bottom graph shows a progressive  $\mu(\tau)$  trend parallel to the  
267 retrograde  $\mu(\tau)$  one for the entire analyzed period, i.e., a continuous tendency of minT  
268 to rise, which becomes significant in 2007, when the progressive  $\mu(\tau)$  assumes values  
269 above  $+1.96$ . On the right, the Sen's slope completes the analysis, illustrating that minT  
270 is increasing at annual level by  $+0.072 \pm 0.011\text{ }^{\circ}\text{C y}^{-1}$ ,  $p < 0.001$ , i.e.,  $+1.44 \pm 0.22\text{ }^{\circ}\text{C}$   
271 over twenty years.

#### 272 *Maximum air temperature (maxT)*

273 The post- and pre-monsoon months show larger increases in maxT, but with lower  
274 magnitudes and significance than we observe for minT (Fig. 4b). The highest increases  
275 for this variable occurs also for maxT in April, November and December. Less expected  
276 is the decrease of maxT in May ( $-0.08\text{ }^{\circ}\text{C y}^{-1}$ ,  $p < 0.05$ ) and during the monsoon months  
277 from June to August ( $-0.05\text{ }^{\circ}\text{C y}^{-1}$ ,  $p < 0.1$ ). On the annual scale, the bottom graph  
278 shows a continuous crossing of the progressive and retrograde  $\mu(\tau)$  trends until 2007,  
279 i.e., a general stationary condition. From 2007 until 2010, the trend significantly  
280 increased, while 2012 and 2013 register a decrease, bringing the progressive  $\mu(\tau)$  near  
281 the stationary condition. In fact, on the right, the Sen's slope confirms that maxT is at  
282 annual level stationary over the twenty years ( $+0.009 \pm 0.012\text{ }^{\circ}\text{C y}^{-1}$ ,  $p > 0.1$ ).

### 283 *Mean air temperature (meanT)*

284 Figure 4c, as expected, presents intermediate conditions for meanT in respect to  
285 minT and maxT. All months, except May and the monsoon months from June and  
286 August, register a positive trend (more or less significant). December presents the  
287 highest a more significant increasing trend ( $+0.17\text{ }^{\circ}\text{C y}^{-1}$ ,  $p < 0.01$ ), while April shows  
288 the highest and a more significant increase ( $p < 0.10$ ) during the pre-monsoon period. On  
289 the annual scale, the bottom graph shows that the progressive  $\mu(\tau)$  trend has always  
290 increased since 2000 and that it becomes significant beginning in 2008. On the right, the  
291 Sen's slope concludes this analysis, showing that meanT has been significantly  
292 increasing by  $+0.044 \pm 0.008\text{ }^{\circ}\text{C y}^{-1}$ ,  $p < 0.05$ , i.e.,  $+0.88 \pm 0.16\text{ }^{\circ}\text{C}$  over twenty years.

### 293 *Total precipitation (Prec)*

294 In the last years, all cells are blue, i.e., we observe for all months an overall and  
295 strongly significant decreasing trend of Prec (Fig. 4d). In general, the post- and pre-  
296 monsoon periods experience more significant decreases, although the monsoon months  
297 (June-September) register the main Prec losses (e.g. August registers a Prec loss of even  
298  $-4.6\text{ mm y}^{-1}$ ). On the annual scale, the bottom graph shows a continuous decreasing  
299 progressive  $\mu(\tau)$  trend since 2000 that becomes significant beginning in 2005. On the  
300 right, the Sen's slope notes that the decreasing Prec trend is strongly high and  
301 significant at annual level ( $-13.7 \pm 2.4\text{ mm y}^{-1}$ ,  $p < 0.001$ ).

302 The precipitation reduction is mainly due to a reduction in intensity (cumulative  
303 precipitation for week). However during the early and late monsoon rather show a  
304 reduction in duration (number of we days for week) (see further details in  
305 Supplementary Material 2).

## 306 5.2 Trend analysis in the Koshi Basin

307 Table 2 provides the descriptive statistics of the Sen's slopes for minT, maxT,  
308 meanT, and Prec for the 1994-2013 period for the Koshi Basin. The stations located on  
309 the two sides of the Himalayan range are listed separately. For the southern ones (KO-  
310 S), we observe that for minT less than half of the stations experience an increasing trend



311 and just three are significant with  $p < 0.1$ . In general, the minT on the southern side can  
312 be defined as stationary ( $+0.003 \text{ }^\circ\text{C y}^{-1}$ ). Conversely, the maxT shows a decidedly non-  
313 stationary condition. All stations present an increasing trend, and even six of the ten are  
314 on the significant rise with at least  $p < 0.1$ . The mean trend is  $+0.060 \text{ }^\circ\text{C y}^{-1}$  ( $p < 0.10$ ).  
315 Similarly, the meanT shows a substantial increase. Also in this case, six of the ten  
316 stations are on the significant rise with at least  $p < 0.1$ . The mean trend is  $+0.029 \text{ }^\circ\text{C y}^{-1}$  ( $p$   
317  $< 0.10$ ). In regards to Prec, we observe that on the KO-S, 14 of the 19 stations present a  
318 downward trend. Among them, eight decrease significantly with at least  $p < 0.1$ . The  
319 mean trend is  $-11.1 \text{ mm y}^{-1}$ , i.e., we observe a decreasing of 15% (222 mm) of precipita-  
320 tion fallen in the basin during the 1994-2013 period (1527 mm on average).

321 The two stations located on the northern ridge (KO-N) show a singularly slight sig-  
322 nificant rise for minT ( $+0.034 \text{ }^\circ\text{C y}^{-1}$ ,  $p < 0.10$  on average) and for maxT ( $+0.039 \text{ }^\circ\text{C y}^{-1}$ ,  
323  $p < 0.10$  on average), recording a consequent mean increase of meanT equal to  $+0.037$   
324  $^\circ\text{C y}^{-1}$ ,  $p < 0.05$ . As for Prec, we observe that on the KO-N both stations maintain sta-  
325 tionary conditions ( $-0.1 \text{ mm y}^{-1}$ ).

326 Table 3 provides the descriptive statistics of the Sen's slopes on a seasonal base. The  
327 stations analyzed here are the same as those considered in Table 2. We begin our  
328 description with PYRAMID, already analyzed in detail in Figure 4. We confirm with  
329 this seasonal grouping that the main and significant increases of minT, maxT, and  
330 meanT are completely concentrated during the post-monsoon period (e.g.,  $+0.124 \text{ }^\circ\text{C y}^{-1}$ ,  
331  $p < 0.01$  for meanT). The pre-monsoon period experienced a slighter and not  
332 significant increase (e.g.,  $+0.035 \text{ }^\circ\text{C y}^{-1}$ ,  $p > 0.1$  for meanT). In general, during the  
333 monsoon period, T is much more stationary for all three variables (e.g.,  $+0.015 \text{ }^\circ\text{C y}^{-1}$ ,  $p$   
334  $> 0.1$  for meanT). Considering the other KO-S stations, the main increasing and  
335 significant trends of meanT occurred during the pre-monsoon ( $+0.043 \text{ }^\circ\text{C y}^{-1}$ ) and post-  
336 monsoon ( $+0.030 \text{ }^\circ\text{C y}^{-1}$ ) season, while the increase during the monsoon is slighter  
337 ( $+0.020 \text{ }^\circ\text{C y}^{-1}$ ). The KO-N stations confirm that the main increasing trend of meanT  
338 occurred outside the monsoon period that is stationary ( $+0.013 \text{ }^\circ\text{C y}^{-1}$ ).

339 As for Prec, PYRAMID and the other KO-S stations show that the magnitude of the  
340 Sen's slopes is higher during the monsoon season ( $-9.3 \text{ mm y}^{-1}$  and  $-8.6 \text{ mm y}^{-1}$ ,  
341 respectively), when precipitation is more abundant. The relatively low snowfall phase of  
342 monsoon Prec at PYRAMID (as specified above) makes the decreasing trend observed  
343 during the summer more robust than the annual one as devoid of the undervaluation of  
344 snowfall, although slight as demonstrated above ( $3\pm 1\%$ ). The northern stations show  
345 slight significant decreasing Prec during the winter ( $-3.3 \text{ mm y}^{-1}$ ,  $p < 0.05$ ).

## 346 5.3 Lapse rates in the southern Koshi Basin

### 347 5.3.1 Air temperature gradient

348 This study, aiming to create a connection between the climate drivers and cryosphere  
349 in the Koshi Basin, which presents the highest altitudinal gradient of the world (77 to  
350 8848 m a.s.l.), offers a unique opportunity to calculate T and Prec lapse rates before

351 analyzing their spatial trends. It is worth noting that the T lapse rate is one of the most  
352 important variables for modeling meltwater runoff from a glacierized basin using the T-  
353 index method (Hock, 2005; Immerzeel et al., 2014). It is also an important variable for  
354 determining the form of Prec and its distribution characteristics (e.g., Hock, 2005).  
355 Figure 5b presents the lapse rate of the annual meanT in the KO Basin (Nepal) along the  
356 altitudinal range of well over 7000 m (865 to 7986 m a.s.l.). We found an altitudinal  
357 gradient of  $-0.60\text{ }^{\circ}\text{C (100 m)}^{-1}$  on the annual scale with a linear trend ( $r^2 = 0.98$ ,  $p <$   
358  $0.001$ ). It is known that up to altitudes of approximately 8-17 km a.s.l. in the lower  
359 regions of the atmosphere, T decreases with altitude at a fairly uniform rate (Washington  
360 and Parkinson, 2005). Considering that the lapse rate is mainly affected by the moisture  
361 content of the air (Washington and Parkinson, 2005), we calculated the seasonal  
362 gradients (not shown here). We found a dry lapse rate of  $-0.65\text{ }^{\circ}\text{C (100 m)}^{-1}$  ( $r^2 = 0.99$ ,  $p$   
363  $< 0.001$ ) during the pre-monsoon season when AWS1 registers a mean relative humidity  
364 of 62%. A saturated lapse rate during the monsoon season is  $-0.57\text{ }^{\circ}\text{C (100 m)}^{-1}$  ( $r^2 =$   
365  $0.99$ ,  $p < 0.001$ ) with a mean relative humidity of 96%. During the post-monsoon  
366 period, we found a lapse rate equal to that registered during the monsoon:  $-0.57\text{ (100}$   
367  $\text{m)}^{-1}$  ( $r^2 = 0.98$ ,  $p < 0.001$ ) even if the relative humidity is decidedly lower in these  
368 months (44%). Kattel and Yao (2013) explain this anomalous low post-monsoon lapse  
369 rate as the effect of strong radiative cooling in winter.

### 370 5.3.2 Precipitation gradient

371 The relationship of Prec with elevation helps in providing a realistic assessment of  
372 water resources and hydrological modeling of mountainous regions (Barros et al.,  
373 2004). In recent years, the spatial variability of Prec has received attention because the  
374 mass losses of the Himalayan glaciers can be explained with an increased variability in  
375 the monsoon system (e.g., Yao et al., 2012; Thakuri et al., 2014).

376 Figure 5a shows the altitudinal gradient for the total annual Prec in the Koshi Basin.  
377 We observe a clear rise in Prec with elevation until approximately 2500 m a.s.l.,  
378 corresponding to the Tarke Ghyang station (code 1058), registering an annual mean of  
379 3669 mm (mean for the 2004-2012 period). A linear approximation ( $r = 0.83$ ,  $p < 0.001$ )  
380 provides a rate of  $+1.16\text{ mm m}^{-1}$ . At higher elevations, we observe an exponential  
381 decrease ( $ae^{bx}$ , with  $a = 21168\text{ mm m}^{-1}$  and  $b = -9\text{ }10^{-4}\text{ m}^{-1}$ , where  $x$  is the elevation  
382 expressed as m a.s.l.) until observing a minimum of 132 mm (years 2009 and 2013) for  
383 the Kala Patthar station (AWS4) at 5600 m a.s.l., although, as specified above, at these  
384 altitudes the contribution of winter snowfall could be slightly underestimated. The  
385 changing point between the two gradients can be reasonably assumed at approximately  
386 2500 m a.s.l., considering that the stations here present the highest interannual  
387 variability, belonging in this way, depending on the year, to the linear increase or to the  
388 exponential decrease. The clear outlier along the linear gradient is the Num Station  
389 (1301) located at 1497 m a.s.l., which recorded 4608 mm of precipitation. This station  
390 has been excluded for the linear approximation because, as reported by Montgomery

391 and Stolar (2006), the station is located in the Arun Valley, which acts as a conduit for  
392 northward transport of monsoonal precipitation. The result is that local precipitation  
393 within the gorge of the Arun River is several times greater than in surrounding areas.

394 Some previous studies of the Himalayas have considered orographic effects on Prec  
395 (Singh and Kumar, 1997; Ichiyanagi et al., 2007). Ichiyanagi et al. (2007), using all  
396 available Prec stations operated by DHM, of which < 5% of stations are located over  
397 2500 m and just one station is over 4000 m a.s.l., observed that in the CH-S region, the  
398 annual Prec increases with altitude below 2000 m a.s.l. and decreases for elevations  
399 ranging between 2000 and 3500 m a.s.l., but with no significant gradient. A broad  
400 picture of the relationship between Prec and topography in the Himalayas can be  
401 derived from the precipitation radar onboard the Tropical Rainfall Measuring Mission  
402 (TRMM). Some authors found an increasing trend with elevation characterized by two  
403 distinct maxima along two elevation bands (950 and 2100 m a.s.l.). The second  
404 maximum is much higher than the first, and it is located along the Lesser Himalayas.  
405 Over these elevations, the annual distribution follows an approximate exponentially  
406 decreasing trend (Bookhagen and Burbank, 2006).

407 Physically, we can interpret the Prec gradient of Fig. 5a considering that when the  
408 humid air masses coming from the Bay of Bengal collide with the orographic barrier,  
409 heavy convections induce huge quantity of rain below 2500 m a.s.l.. The topographic  
410 barrier of the Himalayan mountain range causes the mechanical lift of the humid air, the  
411 cooling of the air column, the condensation and the consequent rainfall. The further  
412 increase in relief induces a depletion of the moisture content resulting in a severe  
413 reduction of Prec at higher altitudes. Our study, based on ground stations, confirms the  
414 general Prec gradient detected with the TRMM microwave observations, even if we did  
415 not identified a marked double maximum Prec peak as observed generally for the whole  
416 central Himalaya by Bookhagen and Burbank, 2006. In fact these author report for our  
417 specific case study (profiles 14 and 15 of their Fig.1(b)) a single step increase in relief  
418 associated with a single Prec maximum.5.4 Spatial distribution of air temperature and  
419 precipitation trends in the Koshi Basin

420 Figure 6 presents the spatial distribution of the Sen's slopes in the Koshi Basin for  
421 minT (Fig. 6a), maxT (Fig. 6b), meanT (Fig. 6c), and Prec (Fig. 6d) during the 1994-  
422 2013 period. The relevant data are reported in Table 2. The Chainpur (East) station  
423 shows T trends in contrast with the other stations (see also Table 2); therefore, we  
424 consider this station as a local anomaly and do not discuss it further in the following  
425 sections.

426 In regards to minT, we observe an overall stationary condition in KO-S, as noted  
427 above. The only two stations showing a significant increasing trend are both located at  
428 East. The high elevation stations (PYRAMID and both those located on the north ridge)  
429 differ from the general pattern of the southern basin by showing a significant increasing  
430 trend. Even for maxT, we observe a higher increase in the southeastern basin. The  
431 central and western parts of the KO-S seem to be more stationary. PYRAMID follows

432 this stationary pattern, while the northern stations (KO-N) show large and significant  
433 increases. As a consequence, meanT shows increasing trends for all the Koshi Basin,  
434 especially on the southeast and northern sides.

435 The decrease of precipitation in the southern Koshi Basin presents a quite  
436 homogeneous pattern from which the highly elevated PYRAMID is not excluded. The  
437 pattern is different on the north ridge, where it is stationary.

## 438 **6 Discussion**

### 439 6.1 Temperature trends of the Koshi Basin compared to the regional pattern

440 The trend analysis carried out in this study for the last two decades in KO-S shows  
441 full consistency with the pattern of change (shown in the following) occurring in these  
442 regions over the last three decades in terms of a higher increase in maxT ( $+0.060\text{ }^{\circ}\text{C y}^{-1}$ )  
443 than in minT ( $+0.003\text{ }^{\circ}\text{C y}^{-1}$ ), a seasonal pattern (more pronounced during the pre- and  
444 post-monsoon months), and the magnitudes of the trends (e.g., the meanT trend is  
445  $+0.030\text{ }^{\circ}\text{C y}^{-1}$ ). Therefore, at low elevations of KO-S, we observe an acceleration of  
446 warming in the recent years compared to the rate of change reported by Kattel and Yao  
447 (2013) and Shrestha et al. (1999) in the previous decades.

448 At regional level, Kattel and Yao (2013) analyzed the annual minT, maxT, and  
449 meanT trends from stations ranging from 1304 m to 2566 m a.s.l. in CH-S (correspond-  
450 ing to all stations in Nepal) during the 1980–2009 period. They found that the magni-  
451 tude of warming is higher for maxT ( $+0.065\text{ }^{\circ}\text{C y}^{-1}$ ), while minT ( $+0.011\text{ }^{\circ}\text{C y}^{-1}$ ) exhib-  
452 its larger variability, such as positive, negative or no change; meanT was found to in-  
453 crease at an intermediate rate of  $+0.038\text{ }^{\circ}\text{C y}^{-1}$ . These authors extended some time series  
454 and confirmed the findings of Shrestha et al. (1999) that, analyzing the 1971–1994 peri-  
455 od, found a maxT increase of  $+0.059\text{ }^{\circ}\text{C y}^{-1}$  for all of Nepal. Furthermore, warming in  
456 the winter was more pronounced compared to other seasons in both studies. These re-  
457 sults are consistent with the pattern reported in WH (e.g., Bhutiyani et al., 2007; Shek-  
458 har et al., 2010), in EH, and in the rest of India (e.g., Pal and Al-Tabbaa, 2010) for the  
459 last three decades.

460 The trend analysis carried out in this study for the last two decades in KO-N agrees  
461 with the regional studies (shown in the following) in regards to both the considerable  
462 increase of minT ( $+0.034\text{ }^{\circ}\text{C y}^{-1}$ ) and the seasonal consistency of trends, related to all  
463 three T variables, outside the monsoon months. However, we observe that in recent  
464 years, maxT is increasing more than the rest of the TP ( $+0.039\text{ }^{\circ}\text{C y}^{-1}$ ). In general we  
465 observed an increase of meanT ( $0.037\text{ }^{\circ}\text{C y}^{-1}$ ) comparable to that reported by Yang et al.  
466 (2012) ( $0.031\text{ }^{\circ}\text{C y}^{-1}$ ) in the 1971–2007 period.

467 At regional level, on the TP, the warming of minT is more prominent than that of  
468 maxT (e.g., Liu et al., 2006; Liu et al., 2009). In particular, for stations above 2000 m  
469 a.s.l. during the 1961–2003 period, Liu et al. (2006) found that minT trends were con-  
470 sistent greater ( $+0.041\text{ }^{\circ}\text{C y}^{-1}$ ) than those of maxT ( $+0.018\text{ }^{\circ}\text{C y}^{-1}$ ), especially in the  
471 winter and spring months. Yang et al. (2012), focusing their analysis on CH-N (which

472 corresponds to the southern TP) in a more recent period (1971–2007), showed a signifi-  
473 cant increase of  $+0.031\text{ }^{\circ}\text{C y}^{-1}$  for meanT. Yang et al. (2006) analyzed five stations lo-  
474 cated in a more limited area of CH-N: the northern side of Mt. Everest (therefore, in-  
475 cluding the two stations also considered in this study) from 1971 to 2004. The warming  
476 is observed to be influenced more markedly by the minT increase.

477 Summarizing PYRAMID shares the higher T trends outside the monsoon period.  
478 However, in contrast with studies located south of the Himalayan ridge, which observed  
479 a prevalence of maxT increase, PYRAMID experienced a consistent minT increase  
480 ( $+0.072\text{ }^{\circ}\text{C y}^{-1}$  for PYRAMID vs  $+0.003\text{ }^{\circ}\text{C y}^{-1}$  for KO-S stations), while the maxT in-  
481 crease is decidedly weaker ( $+0.009\text{ }^{\circ}\text{C y}^{-1}$  for PYRAMID vs  $+0.060\text{ }^{\circ}\text{C y}^{-1}$  for KO-S  
482 stations). The remarkable minT trend of PYRAMID is higher, but more similar to the  
483 pattern of change commonly described on the TP, in particular in CH-N, and also in this  
484 study ( $+0.072\text{ }^{\circ}\text{C y}^{-1}$  for PYRAMID vs  $+0.034\text{ }^{\circ}\text{C y}^{-1}$  for KO-N stations), while the  
485 maxT increase is weaker ( $+0.009\text{ }^{\circ}\text{C y}^{-1}$  for PYRAMID vs  $+0.039\text{ }^{\circ}\text{C y}^{-1}$  for KO-N sta-  
486 tions).

## 487 6.2 Elevation dependency of temperature trends

488 Figure 7 shows T trends in the KO Basin for minT, meanT, and maxT relative to the  
489 elevation during the 1994–2013 period. No linear pattern emerges. However, we can  
490 observe the minT trend of the three stations located at higher altitude (PYRAMID and  
491 KO-N stations), which increases more than that of the lower stations (Fig. 7a, see also  
492 Table 2). Reviewing the most recent studies in the surroundings, we found that they are  
493 quite exclusively located on CH-N. These studies often show contradictory elevation  
494 dependencies (Rangwala and Miller, 2012). A recent study by You et al. (2010) did not  
495 find any significant elevation dependency in the warming rates of meanT between 1961  
496 and 2005. However, considering mostly the same stations, Liu et al. (2009) found that  
497 the warming rates for minT were greater at higher elevations. Observations from CH-S  
498 are much rarer. Shrestha et al. (1999) found elevation dependency in the rate at which  
499 maxT were increasing in the Nepali Himalayas (CH-S), with higher rates at higher  
500 elevations, but this study exclusively considered stations under 3000 m a.s.l.

501 Furthermore we did not find for the Koshi Basin any significant elevation  
502 dependency in the weakening rates of Prec.

## 503 6.3 Precipitation trends of the Koshi Basin compared to the regional pattern

504 As will be detailed in the following, different from the north side of Mt. Everest and  
505 from the general TP, we confirm the general monsoon weakening in the KO-S,  
506 observing a substantial Prec decrease of 15% ( $-11.1\text{ mm y}^{-1}$ ,  $-222\text{ mm}$ ), but that is not  
507 significant for all stations. At PYRAMID, the annual loss is relatively comparable with  
508 that of the KO-S ( $-13.7\text{ mm y}^{-1}$ ,  $-273\text{ mm}$ ), but at these high elevations, as we observed  
509 in Table 2, the weather is much more drier (449 and 1527 mm, respectively). Therefore,  
510 the fractional loss is more than 3 times ( $-52\%$ ) that of the KO-S. Considering that the

511 decreasing trend observed during the summer is more robust than the annual one (see  
512 above), the fractional loss of Prec during the monsoon is -47%, which means that  
513 currently, on average, the precipitation at PYRAMID is the half of what it was twenty  
514 years ago.

515 At regional level, Turner and Annamalai (2012), using the all-India rainfall data  
516 based on a weighted mean of 306 stations, observed a negative precipitation trend since  
517 the 1950s in South Asia. According to Yao et al. (2012), using the Global Precipitation  
518 Climatology Project (GPCP) data, there is strong evidence that precipitation from 1979  
519 to 2010 decreased even in the Himalayas. In eastern CH-S, where the Koshi Basin is  
520 located, they estimated a loss of 173 mm, showing a real decreasing trend starting from  
521 the early 1990s (mean value between grid 9 and 11 in Fig. S18 of their paper).

522 On the TP, the observed pattern of change is opposite that of the monsoon weakening  
523 described by the authors cited above. Liu et al. (2010) described an increase in  
524 precipitation in CH-N for the period of the 1980s to 2008. Su et al. (2006) described a  
525 marked precipitation increase in the Yangtze River Basin (eastern CH-N). In a similar  
526 way to the T analysis, Yang et al. (2006) considered 5 stations located on the northern  
527 side of Mt. Everest (therefore, including the two stations also considered in this study)  
528 from 1971 to 2004 and observed an increasing, but not significant Prec trend. The  
529 higher stationarity we observed is confirmed since 1971 for the two KO-N stations  
530 considered in this study.

#### 531 6.4 Mechanisms responsible for temperature warming and precipitation weakening

532 According to Rangwala and Miller (2012), there are a number of mechanisms that  
533 can cause enhanced warming rates at high elevation, and they often have strong  
534 seasonal dependency. These mechanisms arise from either elevation based differential  
535 changes in climate drivers, such as snow cover, clouds, specific humidity, aerosols, and  
536 soil moisture, or differential sensitivities of surface warming to changes in these drivers  
537 at different elevations. This study does not aim to either realize a comprehensive review  
538 or to demonstrate the causes that could have led to the climate change pattern observed  
539 at PYRAMID, but our intent here is just to note the recent hypotheses advanced in the  
540 literature that fit with our observations for the region of investigation.

541 Snow/ice albedo is one of the strongest feedbacks in the climate system (Rangwala  
542 and Miller, 2012). Increases in minT are possible if decreases in snow cover are  
543 accompanied by increases in soil moisture and surface humidity, which can facilitate a  
544 greater diurnal retention of the daytime solar energy in the land surface and amplify the  
545 longwave heating of the land surface at night (Rangwala et al., 2012). For the Tibetan  
546 Plateau, Rikiishi and Nakasato (2006) found that the length of the snow cover season  
547 declined at all elevations between 1966 and 2001. Moreover, minT can be enhanced by  
548 nighttime increases in cloud cover. However, assessing changes in clouds and  
549 quantifying cloud feedbacks will remain challenging in the near term. For the Tibetan  
550 Plateau, Duan and Wu (2006) found that low level nocturnal cloud cover increased over

551 the TP between 1961 and 2003 and that these increases explain part of the observed  
552 increases in minT.

553 The maxT increase observed here during April ( $p < 0.05$  in 2011, Fig. 4b) fits with  
554 the warming reported by Pal and Al-Tabbaa (2010) which observed that within the pre-  
555 monsoon season only April shows significant changes in maxT in all Indian regions and  
556 WH (1901-2003 period). According to Ramanathan et al. (2007), Gautam et al. (2010)  
557 argued that the observed warming during the pre-monsoon period (April-June) can be  
558 ascribed not only to the global greenhouse warming, but also to the solar radiation ab-  
559 sorption caused by the large amount of aerosol (mineral dust mixed with other carbona-  
560 ceous material) transported over the Gangetic-Himalayan region. As recently reported  
561 by Marinoni et al. (2013), April represents the month for which the transport of absorb-  
562 ing carbonaceous aerosol (i.e. black carbon) is maximized in our region of investigation  
563 (Khumbu Valley). At this regards Putero et al. (2013) show evidences for a possible in-  
564 fluence of open fire occurrence in South Asia particular abundant during this period of  
565 the year. However the significant decreasing of maxT observed in May ( $p < 0.05$ ) and  
566 the slight significant decreasing during the monsoon months from June to August ( $p <$   
567  $0.10$ ) appear to deviate from the scenario proposed for April. In this respect it should be  
568 kept in mind that the radioactive dynamical interactions of aerosol with the monsoon  
569 cycle are extremely complex and different processes can interact with each other. As an  
570 instance, as reported by Qian et al. (2011), the deposition of absorbing aerosol on snow  
571 and the snow albedo feedback processes can play a prominent role in Himalayas and TP  
572 inducing large radioactive flux changes and surface temperature perturbation.

573 Recent studies associate the precipitation decrease over India during the second half  
574 of 20<sup>th</sup> century (e.g., Ramanathan et al., 2005; Lau and Kim, 2006) to the significant  
575 tropospheric warming over the tropical area from the Indian Ocean to the western  
576 Pacific (e.g., Wu, 2005), while westerlies are strengthening (Zhao et al., 2012). Other  
577 authors (e.g., Bolland et al., 2011) attribute the monsoon weakening to human-  
578 influenced aerosol emissions. In fact an increase of aerosols over South Asia has been  
579 well documented (Ramanathan et al., 2005; Lau and Kim, 2006) and climate model  
580 experiments suggest that sulfate aerosol may significantly reduce monsoon precipitation  
581 (Mitchell and Johns, 1997). Despite a historical weakening of the monsoon circulation,  
582 most studies project an increase of the seasonal monsoon rainfall under global warming.  
583 At this regards Levy II et al., 2013 find that the dramatic emission reductions (35%–  
584 80%) in anthropogenic aerosols and their precursors projected by Representative  
585 Concentration Pathway (RCP) 4.5 (Moss et al., 2010) result an increasing trend by the  
586 second half of the 21st century in South Asia and in particular over the Himalaya  
587 (Palazzi et al., 2013).

588 6.5 Linking climate change patterns observed at high elevation with glacier responses

589 *6.5.1 Impact of temperature increase*

590 Air temperature and precipitation are the two factors most commonly related to

591 glacier fluctuations. However, there still exists a seasonal gap in order to explain the  
592 shrinking of summer accumulation-type glaciers (typical of CH) due to large  
593 temperature increases observed in the region during winter (Ueno and Aryal, 2008), as  
594 is the case for the south slopes of Mt. Everest. Furthermore, in this study we noted a  
595 slightly significant decline in summer maxT and stationary meanT. The real increase of  
596 T has been observed for minT, but given the mean elevation of glaciers (5695 m a.s.l. in  
597 1992) and the mean elevation range of glacier fronts (4568-4817 m a.s.l. in 1992, mean  
598 4817 m a.s.l., 249 m of standard deviation –sd-) (Thakuri et al., 2014), this increase for  
599 minT can be most likely considered ineffective for melting processes, since T is still less  
600 than 0 °C. This inference can be ascertained analyzing Figure 8, created in order to link  
601 temperature increases and altitudinal glacier distribution (data from Thakuri et al.,  
602 2014). The 0 °C isotherms, corresponding to the mean monthly minT and maxT, are  
603 plotted for 1994 and 2013. The elevation of each 0 °C isotherm is calculated according  
604 to the accurate lapse rates computation carried out in this study and the observed  
605 monthly T trends. We can note that in 1994 the 0 °C isotherm for minT reached the  
606 elevation band characterizing the glacier fronts only from June to September. However,  
607 twenty years later, the upward of the 0 °C isotherm is modest (+92 m) during these  
608 months, compared to the huge but ineffective rise for melting processes (downstream  
609 from the glacier fronts) of December-November (even +854 m). The maxT has  
610 obviously a greater potential impact on glaciers. In fact the 0 °C isotherm for of all  
611 months except January and February crosses the elevation bands within which the  
612 glacier fronts are located ever since 1994. In this regard we observe that only April  
613 (+224 m), December (+212 m), and November (+160 m) experienced an upward of the  
614 0 °C isotherm able to enhance the melting processes, but only close to the glaciers  
615 fronts. We therefore point out that the impact caused by the increased temperature  
616 occurring in April most likely plays an important role not only in relation to this case  
617 study, but also at the level of the Himalayan range. In fact, as mentioned above, Pal and  
618 Al-Tabbaa (2010), observed that within the pre-monsoon season, only April showed  
619 significant changes in maxT in all Indian regions and WH (1901-2003 period).

#### 620 *6.5.2 Impact of precipitation decrease*

621

622 As regards the precipitation, in this study we noted a strong and significant  
623 decreasing Prec trend for all months, corresponding to a fractional loss of 47% during  
624 the monsoon season which indicates that, on average, the precipitation at PYRAMID is  
625 currently half of what it was twenty years ago. This climate change pattern confirms and  
626 clarifies the observation of Thakuri et al. (2014), who noted that the southern Mt.  
627 Everest glaciers experienced a shrinkage acceleration over the last twenty years (1992-  
628 2011), as underlined by an upward shift of SLA with a velocity almost three times  
629 greater than the previous period (1962-1992). The authors, without the support of  
630 climatic data, proposed the hypothesis that Mt. Everest glaciers are shrinking faster  
631 since the early 1990s mainly as a result of a weakening of precipitation over the last



632 decades. In fact they observed a double upward shift in the SLA of the largest glaciers  
633 (south-oriented and with a higher altitude accumulation zone): a clear signal of a  
634 significant decrease in accumulation. Wagnon et al. (2013) have recently reached the  
635 same conclusion, but also in this case without the support of any climatic studies. Bolch  
636 et al. (2011) and Nuimura et al. (2012) registered a higher mass loss rate during the last  
637 decade (2000–2010).

638 Furthermore Quincey et al. (2009) and Peters et al. (2010) observed lower glacier  
639 flow velocity in the region over the last decades. Many studies highlight how the  
640 present condition of ice stagnation of glaciers in the Mt Everest region, and in general  
641 in CH-S, is attributable to low flow velocity generated by generally negative mass  
642 balances (Bolch et al., 2008; Quincey et al., 2009; Scherler et al., 2011). Our  
643 observations allow attributing the lower glacier flow velocity to lower accumulation due  
644 to weaker precipitation, which can thus be considered the main climatic factor driving  
645 the current ice stagnation of tongues. In this regard we need to keep in mind that  
646 changes in velocity are among the main triggers for the formation of supraglacial and  
647 proglacial lakes (Salerno et al., 2012; Quincey et al., 2009), which we know to be  
648 susceptible to GLOFs.

#### 649 *6.5.3 Trend analysis of annual probability of snowfall*

650 Figure 9 analyses how the changes observed for the meanT at PYRAMID have  
651 affected the probability of snowfall on total cumulated annual precipitation in the last  
652 twenty years. The increase of meanT observed outside the monsoon period, when the  
653 precipitation is almost completely composed by snow (Fig. 2), brought a significant  
654 decrease of solid phase ( $+0.7\% \text{ y}^{-1}$ ,  $p < 0.05$ ). Extending this analysis to the elevation  
655 bands characterizing the glaciers distribution (see Fig. 8), through the temperature lapse  
656 rate calculated here, we observe that at the level of the mean glaciers (5695 m a.s.l.) the  
657 probability of snowfall is stationary ( $+0.04\% \text{ y}^{-1}$ ), while it decreases at the mean  
658 elevation of SLAs (5345 m a.s.l. in 1992, Thakuri et al., 2014), but not significantly ( $-$   
659  $0.38\% \text{ y}^{-1}$ ,  $p > 0.1$ ). The reduction becomes significant at lower altitudes. In particular,  
660 at the mean elevation of glacier fronts (4817 m a.s.l.) the probability of snowfall is  $-0.56$   
661  $\% \text{ y}^{-1}$  ( $p < 0.05$ ), i.e. at these altitudes the probability of snow on annual base is  
662 currently 11 % ( $p < 0.05$ ) less than twenty years ago. We can conclude this analysis  
663 summarizing that a significant change in precipitation phase has occurred close to the  
664 terminal portions of glaciers, corresponding broadly to the glaciers ablation zones  
665 (around 10 %,  $p < 0.5$ ), while the lower temperature of the upper glaciers zones has so  
666 far guaranteed a stationary condition.

#### 667 **Conclusion**

668 Most relevant studies on temperature trends were conducted on the Tibetan Plateau,  
669 the Indian subcontinent (including the WH) and the Upper Indus Basin, while studies  
670 on the mountainous regions along the southern slope of the central Himalayas in Nepal

671 (CH-S) are limited. Although Shrestha et al. (1999) analyzed the maximum temperature  
672 trends over Nepal during the period 1971–1994, studies on recent temperature trends  
673 over CH-S are still lacking and, before this study, completely absent as regards high  
674 elevation. This paper addresses seasonal variability of minimum, maximum, and mean  
675 temperatures and precipitation at high elevation on the southern slopes of Mt. Everest.  
676 Moreover, we complete this analysis with data from all the existing weather stations  
677 located on both sides of the Himalayan range (Koshi Basin) for the 1994-2013 period,  
678 during which a rapider glacier mass loss occurred.

679 At high elevation on the southern slopes of Mt. Everest, we observed the following:

680 1) The main increases in air temperature are almost completely concentrated during  
681 the post-monsoon months. The pre-monsoon period experienced a slighter and  
682 insignificant increase, while the monsoon season is generally stationary. This  
683 seasonal temperature change pattern is shared with the entire Koshi Basin, and it  
684 is also observed in the regional studies related to the northern and southern  
685 slopes of the Himalayan range. Surprisingly, above 5000 m a.s.l. the maximum  
686 temperature decreases significantly in May and slightly during the monsoon  
687 months from June to August.

688 2) The minimum temperature increased much more than the maximum  
689 temperature. This remarkable minimum temperature trend is more similar to the  
690 pattern of change commonly described on the Tibetan Plateau and confirmed in  
691 this study in the northern Koshi Basin. However, this trend is in contrast with  
692 studies located south of the Himalayan ridge. As proved by this study, the  
693 southern Koshi Basin experienced a prevalence of maximum temperature  
694 increases. No linear pattern emerges in the elevation dependency of temperature  
695 trends. We only observed higher minimum temperature trends at higher  
696 altitudes.

697 3) The total annual precipitation has considerably decreased. The annual rate of  
698 decrease above 5000 m a.s.l. is similar to the one at lower altitudes on the  
699 southern side of the Koshi Basin, but the drier conditions of this remote  
700 environment make the fractional loss relatively more consistent. The  
701 precipitation at high elevation during the monsoon period is currently half of  
702 what it was twenty years ago. These observations confirm the monsoon  
703 weakening observed by previous studies in India and even in the Himalayas  
704 since the early 1980s. As opposed to the northern side of the Koshi Basin that  
705 shows in this study certain stability, as positive or stationary trends have been  
706 observed by previous studies on the TP and more specifically in northern central  
707 Himalaya.

708 4) There is a significantly lower probability of snowfall in the glaciers ablation  
709 zones, while the lower temperature of the upper glaciers zones have so far  
710 guaranteed a stationary condition.

711 In general, this study contributes to change the perspective on how the climatic  
712 driver (temperature vs. precipitation) led the glacier responses in the last twenty years.

713 Without demonstrating the causes that could have led to the climate change pattern  
714 observed at the PYRAMID, we simply note the recent literature on hypotheses that  
715 accord with our observations.

716 In conclusion, we have here observed that weather stations at low elevations are not  
717 able to suitably describe the climate changes occurring above 5000 m a.s.l. and thus  
718 correctly interpret the impact observed on the cryosphere. This consideration stresses  
719 the great importance of long-term ground measurements at high elevation.

## 720 **Author contributions**

721 G.T., Y.M. and E.V. designed research; F.S. performed research; F.S., N.G., S.T., G.V.  
722 and E.R. analyzed data; F.S., N.G., E.R. and G.T. wrote the paper. P.C., P.S., N.G. and  
723 G.A. data quality check.

## 724 **Acknowledgements**

725 This work was supported by the MIUR through Ev-K2-CNR/SHARE and CNR-  
726 DTA/NEXTDATA project within the framework of the Ev-K2-CNR and Nepal  
727 Academy of Science and Technology (NAST). Sudeep Thakuri is recipient of the IPCC  
728 Scholarship Award under the collaboration between the IPCC Scholarship Programme  
729 and the Prince Albert II of Monaco Foundation's Young Researchers Scholarships  
730 Initiative.

## 731 **References**

- 732 Abebe, A., Solomatine, D., and Venneker, R.: Application of adaptive fuzzy rule based  
733 models for reconstruction of missing precipitation events, *Hydrolog. Sci. J.*, 45, 425–  
734 436, doi:10.1080/02626660009492339, 2000.
- 735 Abudu, S., Bawazir, A. S., and King, J. P.: Infilling missing daily evapotranspiration  
736 data using neural networks, *J. Irrig. Drain. E-asce*, 136, 317–325,  
737 doi:10.1061/(ASCE)IR.1943-4774.0000197, 2010.
- 738 Amatya, L. K., Cuccillato, E., Haack, B., Shadie, P., Sattar, N., Bajracharya, B.,  
739 Shrestha, B. Caroli, P., Panzeri, D., Basani, M., Schommer, B., Flury, B. Salerno, F.,  
740 and Manfredi, E. C.: Improving communication for management of social-ecological  
741 systems in high mountain areas: Development of methodologies and tools – The  
742 HKKH Partnership Project, *Mt. Res. Dev.*, 30, 69-79, doi:10.1659/MRD-JOURNAL-  
743 D-09-00084.1, 2010.
- 744 Bajracharya B., Uddin, K., Chettri, N., Shrestha, B., and Siddiqui, S. A.: Understanding  
745 land cover change using a harmonized classification system in the Himalayas: A case  
746 study from Sagarmatha National Park, Nepal, *Mt. Res. Dev.*, 30, 143–156, doi:  
747 10.1659/MRD-JOURNAL-D-09-00044.1, 2010.
- 748 Barros, A. P., Kim, G., Williams, E., and Nesbitt, S. W.: Probing orographic controls in  
749 the Himalayas during the monsoon using satellite imagery, *Nat. Hazards Earth Syst.*

750 Sci. 4, 29–51, doi:10.5194/nhess-4-29-2004, 2004.

751 Benn, D. I., Bolch, T., Hands, K., Gulley, J., Luckman, A., Nicholson, L. I., Quincey,  
752 D., Thompson, S., Toumi, R., and Wiseman, S.: Response of debris-covered glaciers  
753 in the Mount Everest region to recent warming, and implications for outburst flood  
754 hazards, *Earth-Sci. Rev.*, 114, 156–174, doi:10.1016/j.earscirev.2012.03.008, 2012.

755 Bertolani L., Bollasina, M., and Tartari, G.: Recent biannual variability of  
756 meteorological features in the Eastern Highland Himalayas, *Geophys. Res. Lett.*, 27,  
757 2185-2188, doi:10.1029/1999GL011198, 2000.

758 Bhutiyani, M. R., Kale, V. S., and Pawar, N. J.: Long-term trends in maximum,  
759 minimum and mean annual air temperatures across the Northwestern Himalaya  
760 during the twentieth century, *Climatic Change*, 85, 159–177, doi:10.1007/s10584-  
761 006-9196-1, 2007.

762 Bocchiola, D. and Diolaiuti, G.: Evidence of climate change within the Adamello  
763 Glacier of Italy, *Theor. Appl. Climatol.*, 100, 351–369, doi:10.1007/s00704-009-  
764 0186-x, 2010.

765 Bolch T., Buchroithner, M., Pieczonka, T., and Kunert, A.: Planimetric and volumetric  
766 glacier changes in the Khumbu Himal, Nepal, since 1962 using Corona, Landsat TM  
767 and ASTER data, *J. Glaciol.*, 54, 592–600, doi: 0.3189/002214308786570782, 2008.

768 Bolch T., Kulkarni, A., Kääh, A., Huggel, C., Paul, F., Cogley, J. G., Frey, H., Kargel, J.  
769 S., Fujita, K., Scheel, M., Bajracharya, S., and Stoffel, M.: The state and fate of  
770 Himalayan glaciers, *Science*, 336, 310-314, doi: 10.1126/science.1215828, 2012.

771 Bolch T., Pieczonka, T., and Benn, D.I.: Multi-decadal mass loss of glaciers in the  
772 Everest area (Nepal Himalaya) derived from stereo imagery, *The Cryosphere*, 5,  
773 349–358, doi:10.5194/tc-5-349-2011, 2011.

774 Bollasina, M. A., Ming, Y., and Ramaswamy, V.: Anthropogenic aerosols and the  
775 weakening of the south Asian summer monsoon, *Science*, 334, 502-505,  
776 doi:10.1126/science.1204994, 2011.

777 Bookhagen, B. and Burbank, D. W.: Topography, relief, and TRMM-derived rainfall  
778 variations along the Himalaya, *Geophys. Res. Lett.*, 33, L08405,  
779 doi:10.1029/2006GL026037, 2006.

780 Carraro, E., Guyennon, N., Hamilton, D., Valsecchi, L., Manfredi, E. C., Viviano, G.,  
781 Salerno, F., Tartari, G., and Copetti, D.: Coupling high-resolution measurements to a  
782 three-dimensional lake model to assess the spatial and temporal dynamics of the  
783 cyanobacterium *Planktothrix rubescens* in a medium-sized lake, *Hydrobiologia*, 698  
784 (1), 77-95. doi:10.1007/s10750-012-1096-y, 2012.

785 Carraro, E., Guyennon, N., Viviano, G., Manfredi, E. C., Valsecchi, L., Salerno, F.,  
786 Tartari, G., and Copetti, D.: Impact of Global and Local Pressures on the Ecology of  
787 a Medium-Sized Pre-Alpine Lake, in *Models of the Ecological Hierarchy*, edited by:  
788 Jordan, F., and Jorgensen, S. E., Elsevier B.V., pp. 259-274, doi:10.1016/B978-0-  
789 444-59396-2.00016-X, 2012b.

790 Coulibaly, P. and Evora, N.: Comparison of neural network methods for infilling  
791 missing daily weather records, *J. Hydrol.*, 341, 27–41,

792 doi:10.1016/j.jhydrol.2007.04.020, 2007.

793 Déqué, M.: Frequency of precipitation and temperature extremes over France in an  
794 anthropogenic scenario: model results and statistical correction according to  
795 observed values, *Global Planet. Change*, 57, 16–26,  
796 doi:10.1016/j.gloplacha.2006.11.030, 2007.

797 Duan, A. and Wu, G.: Change of cloud amount and the climate warming on the Tibetan  
798 Plateau, *Geophys. Res. Lett.*, 33, L22704, doi:10.1029/2006GL027946, 2006.

799 Dytham, C.: *Choosing and Using Statistics: A Biologist's Guide*, John Wiley & Sons,  
800 2011.

801 Fujita, K., and Sakai, A.: Modelling runoff from a Himalayan debris-covered glacier,  
802 *Hydrol. Earth Syst. Sci.*, 18, 2679–2694, doi:10.5194/hess-18-2679-2014, 2014.

803 Fujita, K., Sakai, A., Takenaka, S., Nuimura, T., Surazakov, A. B., Sawagaki, T., and  
804 Yamanokuchi T.: Potential flood volume of Himalayan glacial lakes, *Nat. Hazards*  
805 *Earth Syst. Sci.*, 13, 1827–1839, doi:10.5194/nhessd-1-15-2013, 2013.

806 Ganguly, N. D. and Iyer, K. N.: Long-term variations of surface air temperature during  
807 summer in India, *Int. J. Climatol.*, 29, 735–746, doi:10.1002/joc.1748, 2009.

808 Gardelle, J., Arnaud, Y., and Berthier, E.: Contrasted evolution of glacial lakes along the  
809 Hindu Kush Himalaya mountain range between 1990 and 2009, *Global Planet.*  
810 *Change*, 75, 47–55, doi:10.1016/j.gloplacha.2010.10.003, 2011.

811 Gautam, R., Hsu, N. C. and Lau, K. M.: Premonsoon aerosol characterization and  
812 radiative effects over the Indo-Gangetic plains: implications for regional climate  
813 warming, *J. Geophys. Res.*, 115, D17208, doi:10.1029/2010JD013819, 2010.

814 Gerstengarbe, F. W. and Werner, P. C.: Estimation of the beginning and end of recurrent  
815 events within a climate regime, *Clim. Res.*, 11, 97–107, 1999.

816 Guyennon, N., Romano, E., Portoghesi, I., Salerno, F., Calmanti, S., Petrangeli, A. B.,  
817 Tartari, G., and Copetti, D.: Benefits from using combined dynamical-statistical  
818 downscaling approaches – lessons from a case study in the Mediterranean region,  
819 *Hydrol. Earth Syst. Sc.*, 17, 705–720, doi:10.5194/hess-17-705-2013, 2013.

820 Hock, R.: Glacier melt: a review of processes and their modeling, *Prog. Phys. Geog.*,  
821 29, 362–391, doi:10.1191/0309133305pp453ra, 2005.

822 Ichayanagi, K., Yamanaka, M. D., Muraji, Y., and Vaidya, B. K.: Precipitation in Nepal  
823 between 1987 and 1996, *Int. J. Climatol.*, 27, 1753–1762, doi:10.1002/joc.1492,  
824 2007.

825 Immerzeel, W. W., Petersen, L., Raetelli, S., and Pellicciotti, F.: The importance of  
826 observed gradients of air temperature and precipitation for modeling runoff from a  
827 glacierized watershed in the Nepal Himalayas, *Water Resour. Res.*, 50,  
828 doi:10.1002/2013WR014506, 2014.

829 James, A. L. and Oldenburg, C. M.: Linear and Monte Carlo uncertainty analysis for  
830 subsurface contaminant transport simulation, *Water Resour. Res.*, 33, 2495–2508,  
831 doi:10.1029/97WR01925, 1997.

832 Kattel, D. B. and Yao, T.: Recent temperature trends at mountain stations on the  
833 southern slope of the central Himalayas, *J. Earth Syst. Sci.*, 122, 215–227, doi:

834 10.1007/s12040-012-0257-8, 2013.

835 Kendall, M.G.: Rank Correlation Methods, Oxford University Press, New York, 1975.

836 Kivekas, N., Sun, J., Zhan, M., Kerminen, V. M., Hyvarinen, A., Komppula, M.,  
837 Viisanen, Y., Hong, N., Zhang, Y., Kulmala, M., Zhang, X. C., Deli-Geer, and  
838 Lihavainen, H.: Long term particle size distribution measurements at Mount  
839 Waliguan, a high-altitude site in inland China, *Atmos. Chem. Phys.*, 9, 5461–5474,  
840 doi:10.5194/acp-9-95461-2009, 2009.

841 Lami, A., Marchetto, A., Musazzi, S., Salerno, F., Tartari, G., Guilizzoni, P., Rogora, M.,  
842 and Tartari, G. A.: Chemical and biological response of two small lakes in the  
843 Khumbu Valley, Himalayas (Nepal) to short-term variability and climatic change as  
844 detected by long-term monitoring and paleolimnological methods, *Hydrobiologia*,  
845 648, 189-205, doi:10.1007/s10750-010-0262-3, 2010.

846 Lau, K.-M., and Kim, K.-M.: Observational relationships between aerosol and Asian  
847 monsoon rainfall, and circulation, *Geophys. Res. Lett.*, 33, L21810,  
848 doi: 10.1029/2006GL027546, 2006.

849 Lavagnini, I., Badocco, D., Pastore, P., and Magno, F.: Theil-Sen nonparametric regres-  
850 sion technique on univariate calibration, inverse regression and detection limits, *Ta-*  
851 *lanta*, 87, 180-188, doi:10.1016/j.talanta.2011.09.059, 2011.

852 Levy II, H., L. W., Horowitz, M. D., Schwarzkopf, Y., Ming, J. C., Golaz, V., Naik, and  
853 Ramaswamy, V.: The roles of aerosol direct and indirect effects in past and future  
854 climate change, *J. Geophys. Res.*, 118, 1–12, doi:10.1002/jgrd.50192, 2013.

855 Liu, J., Yang, B., and Qin, C.: Tree-ring based annual precipitation reconstruction since  
856 AD 1480 in south central Tibet. *Quatern. Int.*, 236, 75-81,  
857 doi:10.1016/j.quaint.2010.03.020, 2010.

858 Liu, K., Cheng, Z., Yan, L., and Yin, Z.: Elevation dependency of recent and future min-  
859 imum surface air temperature trends in the Tibetan Plateau and its surroundings,  
860 *Global Planet. Change*, 68, 164–174, doi:10.1016/j.gloplacha.2009.03.017, 2009.

861 Liu, X. D., and Chen, B. D.: Climatic warming in the Tibetan Plateau during recent  
862 decades, *Int. J. Climatol.*, 20, 1729–1742, doi:10.1002/1097-  
863 0088(20001130)20:14<1729::AID-JOC556>3.0.CO;2-Y, 2000.

864 Liu, X.D., Yin, Z. Y., Shao, X., and Qin, N.: Temporal trends and variability of daily  
865 maximum and minimum, extreme temperature events, and growing season length  
866 over the eastern and central Tibetan Plateau during 1961–2003, *J. Geophys. Res.*,  
867 111, D19, doi:10.1029/2005JD006915, 2006.

868 Manfredi, E. C., Flury, B., Viviano, G., Thakuri, S., Khanal, S. N., Jha, P. K., Maskey,  
869 R. K., Kayastha, R. B., Kafle, K. R., Bhochhibhoya, S., Ghimire, N. P., Shrestha, B.  
870 B., Chaudhary, G., Giannino, F., Carteni, F., Mazzoleni, S., and Salerno, F.: Solid  
871 waste and water quality management models for Sagarmatha National Park and  
872 Buffer Zone, Nepal: implementation of a participatory modeling framework, *Mt.*  
873 *Res. Dev.*, 30, 127-142, doi:10.1659/MRD-JOURNAL-D-10-00028.1, 2010.

874 Marinoni, A., Cristofanelli, P., Laj, P., Putero, D., Calzolari, F., Landi, T. C., Vuillermoz,  
875 E., Maione, M., and Bonasoni, P.: High black carbon and ozone concentrations

876 during pollution transport in the Himalayas: Five years of continuous observations at  
877 NCO-Prec global GAW station, *J. Environ. Sci.*, 25, 1618–1625, doi:10.1016/S1001-  
878 0742(12)60242-3, 2013.

879 Menne, M. J., Durre, I., Vose, R. S., Gleason, B. E., and Houston, T. G.: An overview of  
880 the Global Historical Climatology Network—daily database, *J. Atmos. Oceanic.  
881 Technol.*, 29, 897–910, 2012.

882 Mitchell, J. F. B. and Johns, T. C.: On the modification of global warming by sulphate  
883 aerosols. *J. Climate*, 10, 245-267, 1997.

884 Montgomery, D. R. and Stolar, D. B.: Reconsidering Himalayan river anticlines,  
885 *Geomorphology*, 82, 4–15, doi:10.1016/j.geomorph.2005.08.021, 2006.

886 Moss, R. H., et al.: The next generation of scenarios for climate change research and  
887 assessment, *Nature*, 463, 747–756, doi:10.1038/nature08823, 2010.

888 Nuimura, T., Fujita, K., Yamaguchi, S., and Sharma, R. R.: Elevation changes of  
889 glaciers revealed by multitemporal digital elevation models calibrated by GPS survey  
890 in the Khumbu region, Nepal Himalaya, 1992–2008, *J. Glaciol.*, 58, 648–656, doi:  
891 10.3189/2012JoG11J061, 2012.

892 Pal, I. and Al-Tabbaa, A.: Long-term changes and variability of monthly extreme tem-  
893 peratures in India, *Theor. Appl. Climatol.*, 100, 45–56, doi:10.1007/s00704-009-  
894 0167-0, 2010.

895 Palazzi, E., von Hardenberg, J., and Provenzale, A.: Precipitation in the Hindu-Kush  
896 Karakoram Himalaya: Observations and future scenarios, *J. Geophys. Res.*, 118, 85-  
897 100, doi: 10.1029/2012JD018697, 2013.

898 Pepin, N. C. and Lundquist, J. D.: Temperature trends at high elevations: patterns across  
899 the globe, *Geophys. Res. Lett.*, 35, doi:10.1029/2008GL034026, 2008.

900 Peters, J., Bolch, T., Buchroithner, M. F., and Bäßler, M.: Glacier Surface Velocities in  
901 the Mount Everest Area/Nepal using ASTER and Ikonos imagery, *Proceeding of 10th  
902 International Symposium on High Mountain Remote Sensing Cartography,  
903 Kathmandu, Nepal*, 313-320, 2010.

904 Putero, D., T. C., Landi, P., Cristofanelli, A., Marinoni, P., Laj, R., Duchi, F., Calzolari,  
905 G. P., Verza and P. Bonasoni, Influence of open vegetation fires on black carbon and  
906 ozone variability in the southern Himalayas (NCO-P, 5079 m a.s.l.), *Environ. Pollut.*,  
907 184, 597-604, doi: 10.1016/j.envpol.2013.09.035, 2013.

908 Qian, Y., Flanner, M., Leung, L., and Wang, W.: Sensitivity studies on the impacts of  
909 Tibetan plateau snowpack pollution on the Asian hydrological cycle and monsoon  
910 climate, *Atmos. Chem. Phys.*, 11, 1929–1948, doi:10.5194/acp-11-1929-2011, 2011.

911 Quincey, D. J., Luckman, A., and Benn, D.: Quantification of Everest region glacier ve-  
912 locities between 1992 and 2002, using satellite radar interferometry and feature  
913 tracking, *J. Glaciol.*, 55, 596-606, doi: 10.3189/002214309789470987, 2009.

914 Ramanathan, V., Chung, C., Kim, D., Bettge, T., Buja, L., Kiehl, J. T., Washington, W.  
915 M., Fu, Q., Sikka, D. R., and Wild, M.: Atmospheric brown clouds: Impacts on South  
916 Asian climate and hydrological cycle. *Proc. Natl. Acad. Sci. U.S.A.*, 102, 5326- 5333,  
917 doi: 10.1073/pnas.0500656102, 2005.

- 918 Ramanathan, V., Li, F., Ramana, M. V., Praveen, P. S., Kim, D., Corrigan, C. E.,  
919 Nguyen, H., Stone, E. A., Schauer, J. J., Carmichael, G. R., Adhikary, B., and Yoon,  
920 S. C.: Atmospheric brown clouds: Hemispherical and regional variations in long-  
921 range transport, absorption, and radiative forcing, *J. Geophys. Res.*, 112, D22,  
922 doi:10.1029/2006JD008124, 2007.
- 923 Rangwala, I. and Miller, J. R.: Climate change in mountains: a review of elevation-  
924 dependent warming and its possible causes, *Climatic Change*, 114, 527–547,  
925 doi:10.1007/s10584-012-0419-3, 2012.
- 926 Rangwala, I., Barsugli, J., Cozzetto, K., Neff, J., and Prairie, J.: Mid-21st century  
927 projections in temperature extremes in the southern Colorado Rocky Mountains from  
928 regional climate models, *Clim Dyn.*, 39, 1823-1840, doi:10.1007/s00382- 011-1282-  
929 z, 2012.
- 930 Rikiishi, K. and Nakasato, H.: Height dependence of the tendency for reduction in  
931 seasonal snow cover in the Himalaya and the Tibetan Plateau region, 1966–2001,  
932 *Ann. Glaciol.*, 43, 369–377, doi: <http://dx.doi.org/10.3189/172756406781811989>,  
933 2006.
- 934 Salerno, F., Buraschi, E., Bruccoleri, G., Tartari, G., and Smiraglia, C.: Glacier surface-  
935 area changes in Sagarmatha National Park, Nepal, in the second half of the 20th cen-  
936 tury, by comparison of historical maps, *J. Glaciol.*, 54, 738-752, 2008.
- 937 Salerno, F., Cuccillato, E., Caroli, P., Bajracharya, B., Manfredi, E. C., Viviano, G.,  
938 Thakuri, S., Flury, B., Basani, M., Giannino, F., and Panzeri, D.: Experience with a  
939 hard and soft participatory modeling framework for social ecological system man-  
940 agement in Mount Everest (Nepal) and K2 (Pakistan) protected areas, *Mt. Res. Dev.*,  
941 30, 80-93, 2010a.
- 942 Salerno, F., Gambelli, S., Viviano, G., Thakuri, S., Guyennon, N., D’Agata, C.,  
943 Diolaiuti, G., Smiraglia, C., Stefani, F., Bochhiola, D., and Tartari, G.: High alpine  
944 ponds shift upwards as average temperature increase: A case study of the Ortles-  
945 Cevedale mountain group (Southern alps, Italy) over the last 50 years, *Global Planet.*  
946 *Change*, doi: 10.1016/j.gloplacha.2014.06.003, 2014.
- 947 Salerno, F., Thakuri, S., D’Agata, C., Smiraglia, C., Manfredi, E. C., Viviano, G., and  
948 Tartari, G.: Glacial lake distribution in the Mount Everest region: Uncertainty of  
949 measurement and conditions of formation, *Global Planet. Change*, 92-93, 30-39,  
950 doi:10.1016/j.gloplacha.2012.04.001, 2012.
- 951 Salerno, F., Viviano, G., Mangredi, E. C., Caroli, P., Thakuri, S., and Tartari, G.: Multi-  
952 ple Carrying Capacities from a management-oriented perspective to operationalize  
953 sustainable tourism in protected area, *J. Environ. Manage.*, 128, 116-125,  
954 doi:10.1016/j.jenvman.2013.04.043, 2013.
- 955 Salerno, F., Viviano, G., Thakuri, S., Flury, B., Maskey, R. K., Khanal, S. N., Bhujju, D.,  
956 Carrer, M., Bhochohibhoya, S., Melis, M. T., Giannino, F., Staiano, A., Carteni, F.,  
957 Mazzoleni, S., Cogo, A., Sapkota, A., Shrestha, S., Pandey, R. K., and Manfredi, E.  
958 C.: Energy, forest, and indoor air pollution models for Sagarmatha National Park and  
959 Buffer zone, Nepal: implementation of a participatory modeling framework, *Mt. Res.*



960 Dev., 30, 113–126, 2010b.

961 Scherler, D., Bookhagen, B., and Strecker, M. R.: Spatially variable response of Hima-  
 962 layan glaciers to climate change affected by debris cover. *Nature Geosci.*, 4, 156–  
 963 159, doi:10.1038/ngeo1068, 2011.

964 Schneider, T.: Analysis of incomplete climate data: Estimation of mean values and  
 965 covariance matrices and imputation of missing values, *J. Clim.*, 14, 853–871,  
 966 doi:10.1175/1520-0442(2001)014<0853:AOICDE>2.0.CO;2, 2001.

967 Sellegri, K., Laj, P., Venzac, H., Boulon, J., Picard, D., Villani, P., Bonasoni, P.,  
 968 Marinoni, A., Cristofanelli, P., and Vuillermoz, E.: Seasonal variations of aerosol size  
 969 distributions based on long-term measurements at the high altitude Himalayan site of  
 970 Nepal Climate Observatory—Pyramid (5079 m), Nepal, *Atmos. Chem. Phys.*, 10,  
 971 10679–10690, doi:10.5194/acp-10.10679-2010, 2010.

972 Sen, P. K.: Estimates of the regression coefficient based on Kendall’s Tau, *J. Am.*  
 973 *Assoc.*, 63, 1379-1389, doi:10.2307/2285891, 1968.

974 Shekhar, M. S., Chand, H., Kumar, S., Srinivasan, K., and Ganju, A.: Climate-change  
 975 studies in the western Himalaya, *Ann. Glaciol.*, 51, 105-112,  
 976 doi:10.3189/172756410791386508, 2010.

977 Shrestha, A. B., Wake, C. P., Mayewski, P. A., and Dibb, J. E.: Maximum temperature  
 978 trends in the Himalaya and its vicinity: An analysis based on temperature records  
 979 from Nepal for the period 1971-94, *J. Clim.*, 12, 2775-5561, doi:10.1175/1520-  
 980 0442(1999)012<2775:MTTITH>2.0.CO;2, 1999.

981 Singh, P. and Kumar, N.: Effect of orography on precipitation in the western Himalayan  
 982 region, *J. Hydrol.*, 199, 183-206, doi:10.1016/S0022-1694(96)03222-2, 1997.

983 Su, B. D., Jiang, T., and Jin, W. B.: Recent trends in observed temperature and  
 984 precipitation extremes in the Yangtze River basin, China, *Theor. Appl. Climatol.*, 83,  
 985 139–151, doi:10.1007/s00704-005-0139-y, 2006.

986 Tartari, G., Salerno, F., Buraschi, E., Bruccoleri, G., and Smiraglia, C.: Lake surface  
 987 area variations in the North-Eastern sector of Sagarmatha National Park (Nepal) at  
 988 the end of the 20th Century by comparison of historical maps, *J. Limnol.*, 67, 139-  
 989 154, doi:10.4081/jlimnol.2008.139, 2008.

990 Tartari, G., Verza, P., and Bertolami, L.: Meteorological data at PYRAMID Observatory  
 991 Laboratory (Khumbu Valley, Sagarmatha National Park, Nepal), in *Limnology of*  
 992 *high altitude lakes in the Mt. Everest Region (Nepal)*, edited by: Lami, A. and  
 993 Giussani, G., *Mem. Ist. Ital. Idrobiol.*, 57, 23-40, 2002.

994 Tartari, G., Vuillermoz, E., Manfredi, E. C., and Toffolon, R.: CEOP High Elevations  
 995 Initiative, *GEWEX News, Special Issue*, 19(3), 4-5, 2009.

996 Thakuri, S., Salerno, F., Smiraglia, C., Bolch, T., D’Agata, C., Viviano, G., and Tartari,  
 997 G.: Tracing glacier changes since the 1960s on the south slope of Mt. Everest (central  
 998 southern Himalaya) using optical satellite imagery, *The Cryosphere*, 8, 1297-1315,  
 999 doi:10.5194/tc-8-1297-2014, 2014.

1000 Themeßl, M. J., Gobiet, A., and Heinrich, G.: Empirical-statistical downscaling and  
 1001 error correction of regional climate models and its impact on the climate change

1002 signal, *Climatic Change*, 112, 449-468, doi:10.1007/s10584-011-011-0224-4, 2012.

1003 Turner, A. G. and Annamalai, H.: Climate change and the South Asian summer  
1004 monsoon, *Nat. Clim. Change*, 2, 587-595, doi:10.1038/nclimate1495, 2012.

1005 Ueno K. and Aryal, R.: Impact of tropical convective activity on monthly temperature  
1006 variability during non monsoon season in the Nepal Himalayas, *J. Geophys. Res.*,  
1007 113, D18112, doi:10.1029/2007JD009524, 2008.

1008 Ueno, K., Endoh, N., Ohata, T., Yabuki, H., Koike, M., and Zhang, Y.: Characteristics of  
1009 precipitation distribution in Tangula, Monsoon, 1993, *Bulletin of Glaciological  
1010 Research*, 12, 39-46, 1994.

1011 UNEP (United Nations Environment Programme)/WCMC (World Conservation  
1012 Monitoring Centre): Sagarmatha National Park, Nepal, in *Encyclopedia of Earth*,  
1013 edited by: McGinley, M. and Cleveland, C. J., Environmental Information Coalition,  
1014 National Council for Science and the Environment, Washington, DC, 2008.

1015 Venzac, H., Sellegri, K., Laj, P., Villani, P., Bonasoni, P., Marinoni, A., Cristofanelli, P.,  
1016 Calzolari, F., Fuzzi, S., Decesari, S., Facchini, M. C., Vullermoz, E., and Verza, G. P.:  
1017 High frequency new particle formation in the Himalayas, *Proc. Natl. Acad. Sci.  
1018 USA*, 105, 15666-15671, doi:10.1073/pnas.0801355105, 2008.

1019 Vuille, M.: Climate variability and high altitude temperature and precipitation, in  
1020 *Encyclopedia of snow, ice and glaciers*, edited by: Singh, V. P. et al., Springer, pp.  
1021 153-156, 2011.

1022 Wagnon, P., Vincent, C., Arnaud, Y., Berthier, E., Vuillermoz, E., Gruber, S., Ménégoz,  
1023 M., Gilbert, A., Dumont, M., Shea, J. M., Stumm, D., and Pokhrel, B. P.: Seasonal  
1024 and annual mass balances of Mera and Pokalde glaciers (Nepal Himalaya) since  
1025 2007, *The Cryosphere*, 7, 1769-1786, doi:10.5194/tc-7-1769-2013, 2013.

1026 Washington, W. M. and Parkinson, C. L.: *An introduction to three-Dimensional Climate  
1027 Modeling*, 2<sup>nd</sup> Edition, University Science Books, Sausalito, 2005.

1028 Wu, B.: Weakening of Indian summer monsoon in recent decades, *Adv. Atmos. Sci.*  
1029 22(1), 21-29, doi:10.1007/BF02930866, 2005.

1030 Yang J., Tan, C., and Zhang, T.: Spatial and temporal variations in air temperature and  
1031 precipitation in the Chinese Himalayas during the 1971–2007, *Int. J. Climatol.*, 33,  
1032 2622-2632, doi:10.1002/joc.3609, 2012.

1033 Yang, X., Zhang, Y., Zhang, W., Yan, Y., Wang, Z., Ding, M., and Chu, D.: Climate  
1034 change in Mt. Qomolangma region since 1971, *J. Geogr. Sci.*, 16, 326-336,  
1035 doi:10.1007/s11442-006-0308-7, 2006.

1036 Yao, T., Thompson, L., Yang, W., Yu, W., Gao, Y., Guo, X., Yang, X., Duan, K., Zhao,  
1037 H., Xu, B., Pu, J., Lu, A., Xiang, Y., Kattel, D. B., and Joswiak, D.: Different glacier  
1038 status with atmospheric circulations in Tibetan Plateau and surroundings, *Nat. Clim.  
1039 Change*, 2, 663-667, doi:10.1038/nclimate1580, 2012.

1040 Yasutomi, N., Hamada, A., and Yatagai, A.: Development of a long-term daily gridded  
1041 temperature dataset and its application to rain/snow discrimination of daily  
1042 precipitation, *Global Environ. Res.*, V15N2, 165-172, 2011.

1043 You, Q., Kang, S., Pepin, N., Flügel, W., Yan, Y., Behrawan, H., and Huang, J.: Rela-

1044 tionship between temperature trend magnitude, elevation and mean temperature in  
1045 the Tibetan Plateau from homogenized surface stations and reanalysis data, *Global*  
1046 *Planet. Change*, 71, 124-133, doi:10.1016/j.gloplacha.2010.01.020, 2010.  
1047 Zhao, H., Xu, B., Yao, T., Wu, G., Lin, S., Gao, J., and Wang, M.: Deuterium excess  
1048 record in a southern Tibetan ice core and its potential climatic implications, *Clim.*  
1049 *Dyn.*, 38, 1791-1803, doi:10.1007/s00382-011-1161-7, 2012.  
1050  
1051

1052 *Table 1. List of surface stations belonging to PYRAMID Observatory Laboratory*  
 1053 *network located along the south slopes of Mt. Everest (upper DK Basin).*

Station ID	Location	Latitude °N	Longitude °E	Elevation m a.s.l.	Sampling Frequency	Data Availability		% of daily missing data	
						From	To	Air Temperature	Precipitation
AWS3	Lukla	27.70	86.72	2660	1 hour	02/11/2004	31/12/2012	23	20
AWSN	Namche	27.80	86.71	3570	1 hour	27/10/2001	31/12/2012	21	27
AWS2	Pheriche	27.90	86.82	4260	1 hour	25/10/2001	31/12/2013	15	22
AWS0	Pyramid	27.96	86.81	5035	2 hours	01/01/1994	31/12/2005	19	16
AWS1	Pyramid	27.96	86.81	5035	1 hour	01/01/2000	31/12/2013	10	21
ABC	Pyramid	27.96	86.82	5079	1 hour	01/03/2006	31/12/2011	5	1
AWS4	Kala Patthar	27.99	86.83	5600	10 minutes	01/01/2009	31/12/2013	28	38
AWS5	South Col	27.96	86.93	7986	10 minutes	01/05/2008	31/10/2011	39	100

1054

1055

1056 Table 2. List of ground weather stations located in the Koshi Basin and descriptive  
 1057 statistics of the Sen's slopes for minimum, maximum, and mean air temperatures and  
 1058 total precipitation for the 1994-2012 period. The annual mean air temperature, the total  
 1059 annual mean precipitation, and the percentage of missing daily values is also reported.  
 1060 Level of significance ( $^{\circ}$   $p$ -value = 0.1, \*  $p$ -value = 0.05, \*\*  $p$ -value = 0.01, and \*\*\*  $p$ -  
 1061 value = 0.001).

ID	Station Name	Latitude	Longitude	Elevation	Air Temperature					Precipitation					
					Annual mean	Missing values	MinT trend	MaxT Trend	MeanT trend	Annual total	Missing values	Prec trend			
					$^{\circ}$ C	%	$^{\circ}$ C $a^{-1}$	$^{\circ}$ C $a^{-1}$	$^{\circ}$ C $a^{-1}$	mm	%	mm $a^{-1}$			
		$^{\circ}$ N	$^{\circ}$ N	m a.s.l.											
KO-S (NEPAL)	1024 DHULIKHEL	27.61	85.55	1552	17.1	2	-0.012	0.041	0.026						
	1036 PANCHKHAL	27.68	85.63	865	21.4	10	0.038	0.051 *	0.038 $^{\circ}$	1191	10	-25.0 *			
	1058 TARKE GHYANG	28.00	85.55	2480						3669	10	-21.9			
	1101 NAGDAHA	27.68	86.10	850						1369	3	-1.4			
	1103 JIRI	27.63	86.23	2003	14.4	1	0.013	0.020	0.014 $^{\circ}$	2484	4	6.6			
	1202 CHAURIKHARK	27.70	86.71	2619						2148	2	1.3			
	1206 OKHALDHUNGA	27.31	86.50	1720	17.6	2	-0.017	0.042	0.000	1786	3	-5.1			
	1210 KURULE GHAT	27.13	86.41	497						1017	2	-23.4 $^{\circ}$			
	1211 KHOTANG BAZAR	27.03	86.83	1295						1324	4	15.9			
	1222 DIKTEL	27.21	86.80	1623						1402	6	10.4			
	1301 NUM	27.55	87.28	1497						4537	6	-54.3 **			
	1303 CHAINPUR (EAST)	27.28	87.33	1329	19.1	0	-0.127 *	0.024	-0.064 $^{\circ}$	1469	0	-1.1			
	1304 PAKHRIBAS	27.05	87.28	1680	16.7	0	-0.005	0.036 *	0.015	1540	4	-3.7			
	1307 DHANKUTA	26.98	87.35	1210	20.0	0	-0.002	0.153 ***	0.071 ***	942	6	-9.2 $^{\circ}$			
	1314 TERHATHUM	27.13	87.55	1633	18.2	10	0.033	0.066 $^{\circ}$	0.049 *	1052	6	-13.1 $^{\circ}$			
	1317 CHEPUWA	27.46	87.25	2590						2531	5	-41.9 *			
	1322 MACHUWAGHAT	26.96	87.16	158						1429	6	-22.9 $^{\circ}$			
	1403 LUNGTHUNG	27.55	87.78	1780						2347	1	2.6			
	1405 TAPLEJUNG	27.35	87.66	1732	16.6	1	0.060 *	0.085 **	0.071 **	1966	3	-11.6			
1419 PHIDIM	27.15	87.75	1205	21.2	7	0.047 *	0.082 **	0.067 **	1287	2	-13.6 *				
	MEAN	27.33	87.00	1587	17.9	2	0.003	0.060 $^{\circ}$	0.029 $^{\circ}$	1527	4	-11.1			
	PYRAMID	27.96	86.81	5035	-2.4	0	0.072 ***	0.009	0.044 *	449	0	-13.7 ***			
KO-N (TIBET)	DINGRI	28.63	87.08	4,302	3.5	0	0.037 $^{\circ}$	0.041 $^{\circ}$	0.037 *	309	0	-0.1			
	NYALAM	28.18	85.97	3,811	4.1	0	0.032 $^{\circ}$	0.036 $^{\circ}$	0.036 $^{\circ}$	616	0	-0.2			
	MEAN	28.41	86.53	4,057	3.8	0.1	0.034 $^{\circ}$	0.039 *	0.037 *	463	0	-0.1			

1062

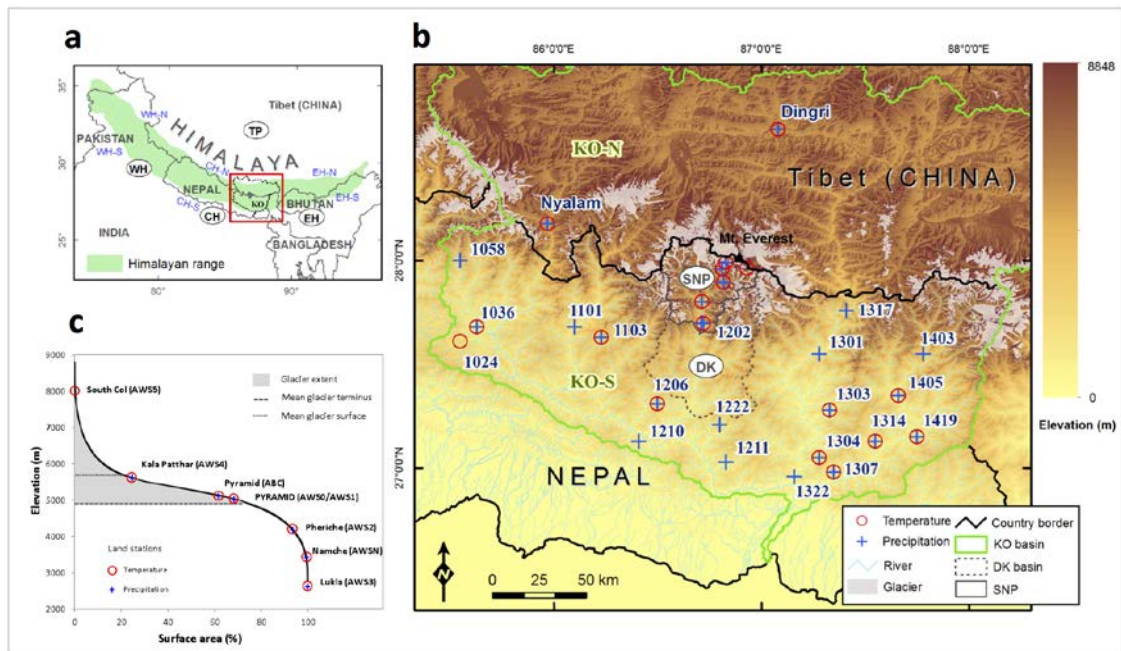
1063

1064 *Table 3. Descriptive statistics of the Sen's slopes on a seasonal basis for minimum,*  
 1065 *maximum, and mean air temperatures and total precipitation of weather stations*  
 1066 *located in the Koshi Basin for the 1994-2012 period. The Nepali and Tibetan stations*  
 1067 *are aggregated as mean values. Level of significance ( $^{\circ}$   $p$ -value = 0.1, \*  $p$ -value = 0.05,*  
 1068 *\*\*  $p$ -value = 0.01, and \*\*\*  $p$ -value = 0.001). Annual and seasonal temperature trends*  
 1069 *are expressed as  $^{\circ}\text{C y}^{-1}$ . Annual precipitation trend is expressed as  $\text{mm y}^{-1}$ , while the*  
 1070 *seasonal precipitation trends are in  $\text{mm (4 months) y}^{-1}$ .*

Location	Minimum Temperature				Maximum Temperature				Mean Temperature				Total Precipitation			
	Pre-	Monsoon	Post-	Annual	Pre-	Monsoon	Post-	Annual	Pre-	Monsoon	Post-	Annual	Pre-	Monsoon	Post-	Annual
SOUTHERN KOSHI BASIN (KO-S, NEPAL)	0.012	-0.005	-0.001	0.003	0.076 <sup>*</sup>	0.052	0.069 <sup>*</sup>	0.060 <sup>*</sup>	0.043	0.020	0.030	0.030 <sup>*</sup>	0.8	-8.6	-2.5	-11.1
PYRAMID (NEPAL)	0.067 <sup>*</sup>	0.041 <sup>*</sup>	0.151 <sup>***</sup>	0.072 <sup>***</sup>	0.024	-0.028	0.049	0.009	0.035	0.015	0.124 <sup>**</sup>	0.044 <sup>**</sup>	-2.5 <sup>**</sup>	-9.3 <sup>**</sup>	-1.4 <sup>**</sup>	-13.7 <sup>***</sup>
NORTHERN KOSHI BASIN (KO-N,TIBET)	0.042 <sup>*</sup>	0.019	0.086 <sup>*</sup>	0.034 <sup>*</sup>	0.023	0.030	0.071 <sup>*</sup>	0.039 <sup>*</sup>	0.042 <sup>*</sup>	0.013	0.084 <sup>*</sup>	0.037 <sup>*</sup>	2.2	0.4	-3.3 <sup>*</sup>	-0.1

1071

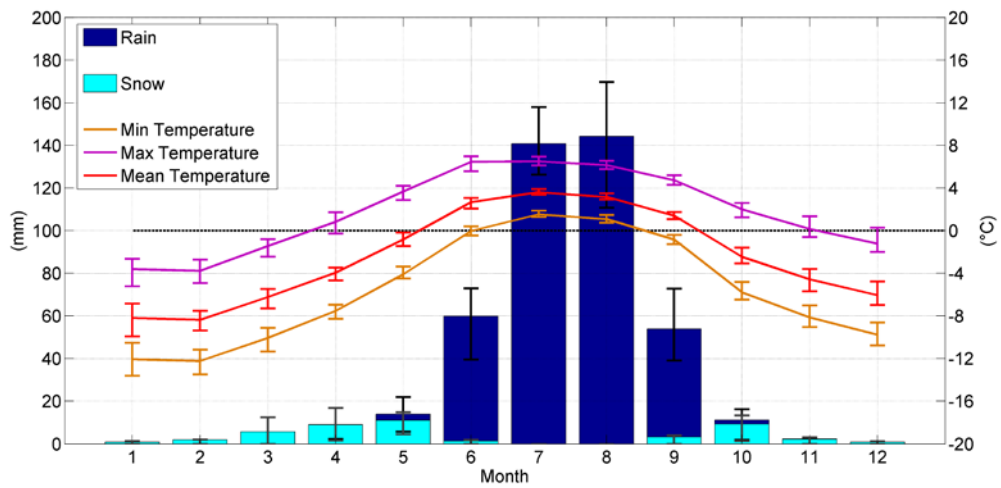
1072



1073

1074 *Figure 1. a) Location of the study area in the Himalaya, where the abbreviations WH,*  
 1075 *CH, EH represents the Western, Central and Eastern Himalaya, respectively (the*  
 1076 *suffixes -N and -S indicate the northern and southern slopes). b) Focused map on the*  
 1077 *spatial distribution of all meteorological stations used in this study, where KO and DK*  
 1078 *stand for the Koshi and Dudh Koshi Basins, respectively; SNP represents the*  
 1079 *Sagarmatha National Park. c) Hypsometric curve of SNP (upper DK Basin) and*  
 1080 *altitudinal glacier distribution. Along this curve, the locations of meteorological*  
 1081 *stations belonging to PYRAMID Observatory Laboratory are presented.*

1082

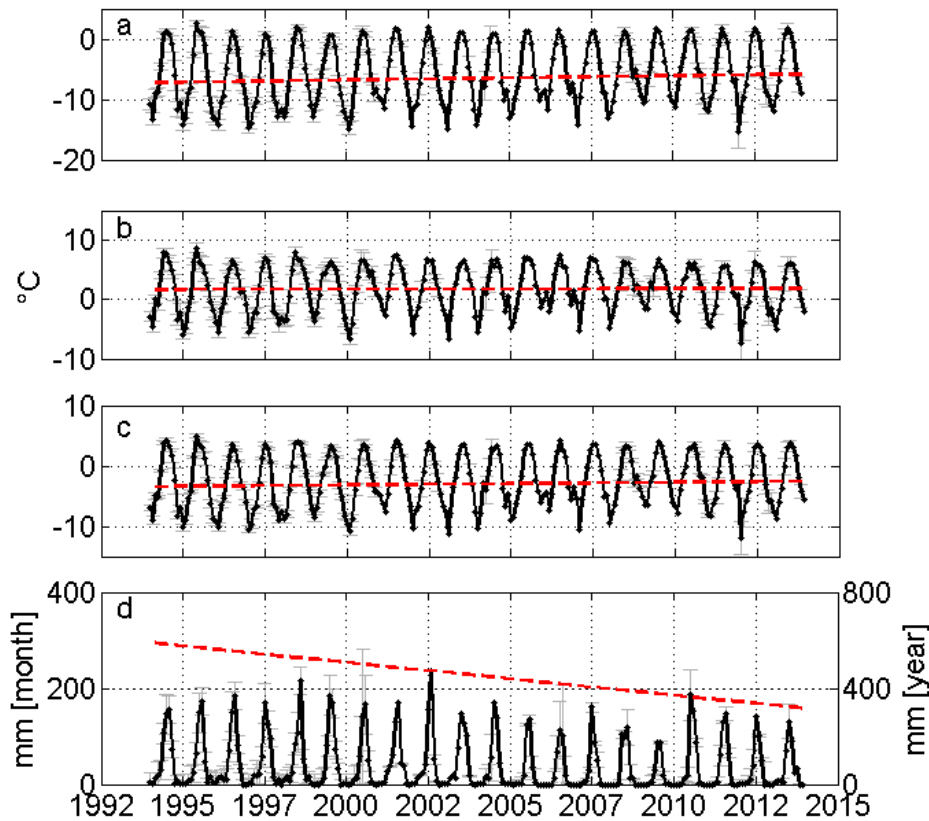


1083

1084 *Figure 2. Mean monthly cumulated precipitation subdivided into snowfall and rainfall*  
 1085 *and minimum, maximum, and mean temperature at 5050 m a.s.l. (reference period*  
 1086 *1994-2013). The bars represent the standard deviation.*

1087

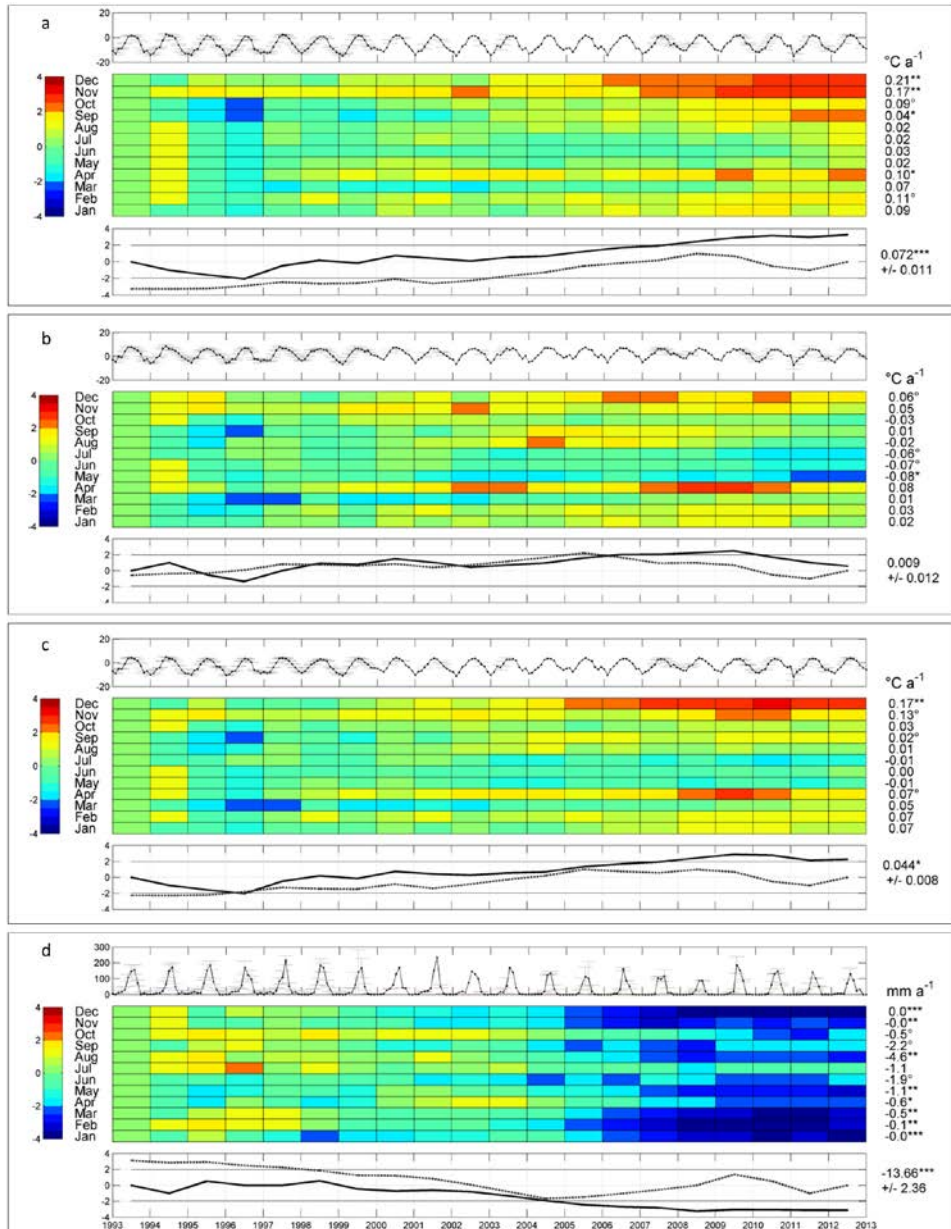




1088

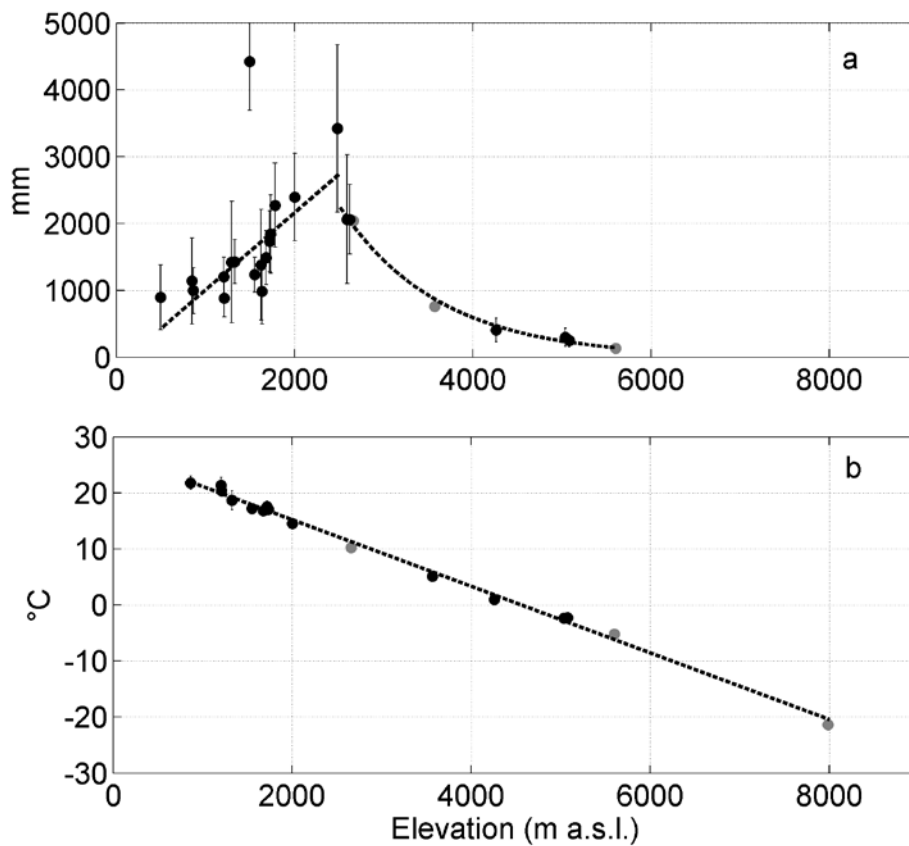
1089 *Figure 3. Temperature and precipitation monthly time series (1994-2013) reconstructed*  
 1090 *at high elevations of Mt. Everest (PYRAMID): minimum (a), maximum (b), and mean*  
 1091 *temperature (c), and precipitation (d). Uncertainty at 95% is presented as gray bar. The*  
 1092 *red lines represents the robust linear fitting of the time series characterized by the*  
 1093 *associated Sen's slope. According to Dytham (2011), the intercepts are calculated by*  
 1094 *taking the slopes back from every observation to the origin. The intercepts used in here*  
 1095 *represent the median values of the intercepts calculated for every point (Lavagnini et*  
 1096 *al., 2011). For precipitation the linear fitting refers at the right axis.*

1097



1098

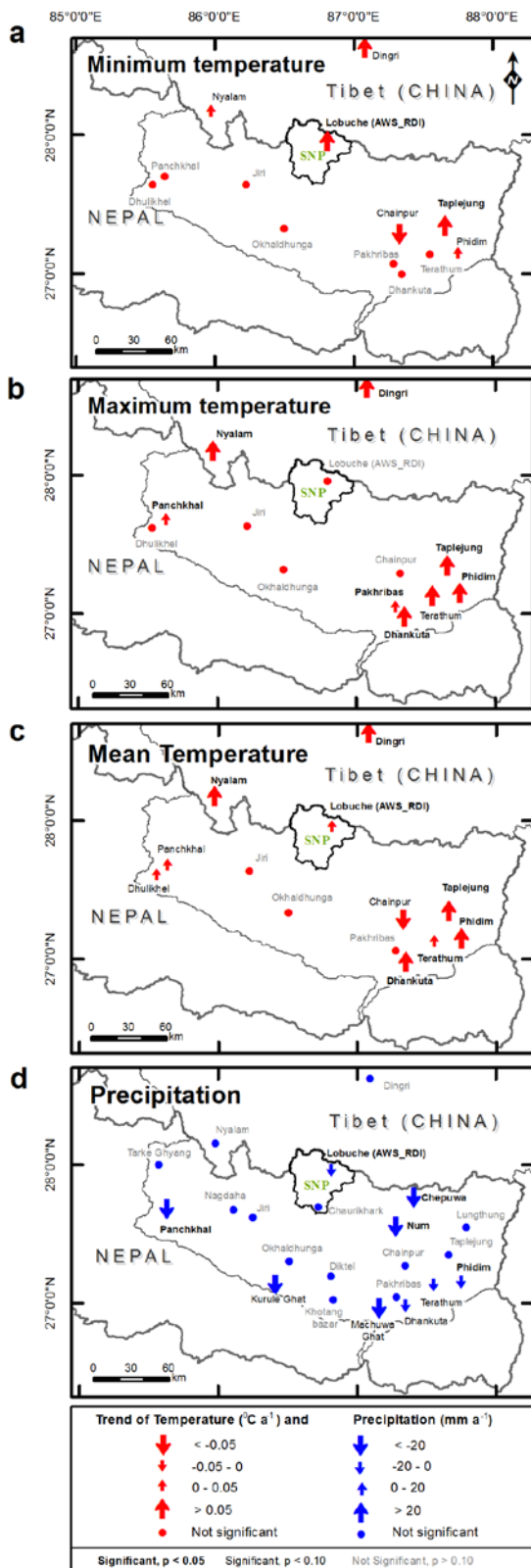
1099 *Figure 4. Trend analysis for a) minimum, b) maximum, and c) mean air temperatures*  
 1100 *and d) total precipitation in the upper DK Basin. The top graph of each meteorological*  
 1101 *variable shows the monthly trend (dark line) and uncertainty due to the reconstruction*  
 1102 *process (gray bars). The central grid displays the results of the sequential Mann-*  
 1103 *Kendall (seqMK) test applied at the monthly level. On the left, the color bar represents*  
 1104 *the normalized Kendall's tau coefficient  $\mu(\tau)$ . The color tones below  $-1.96$  and above*  
 1105  *$1.96$  are significant ( $\alpha = 5\%$ ). On the right, the monthly Sen's slopes and the relevant*  
 1106 *significance levels for the 1994-2013 period ( $^{\circ}$   $p$ -value = 0.1, \*  $p$ -value = 0.05, \*\*  $p$ -*  
 1107 *value = 0.01, and \*\*\*  $p$ -value = 0.001). The bottom graph plots the progressive (black*  
 1108 *line) and retrograde (dotted line)  $\mu(\tau)$  applied on the annual scale. On the right, the*  
 1109 *annual Sen's slope is shown for the 1994-2013 period. [MATLAB® script is available at](http://www.irs.cnr.it/Docs/Code/MSeqMK.m)*  
 1110 *<http://www.irs.cnr.it/Docs/Code/MSeqMK.m>*



1111

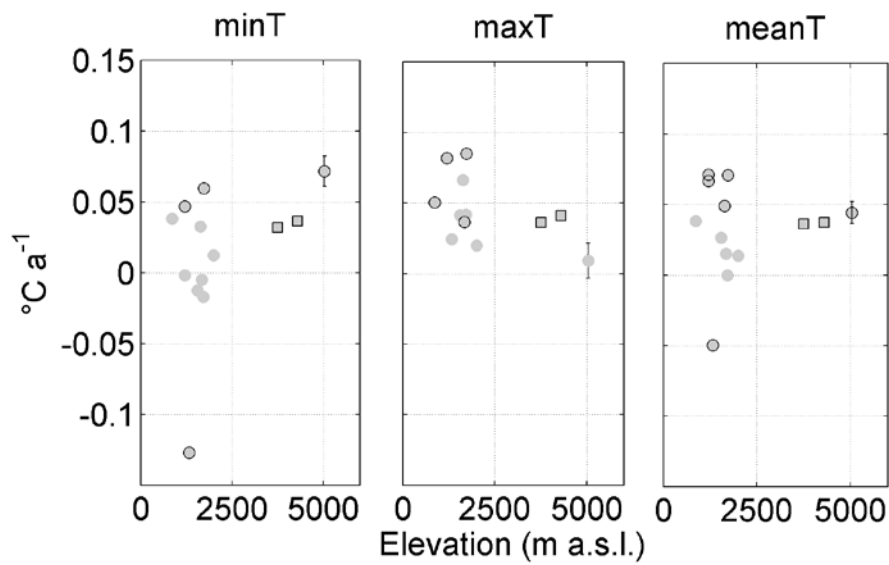
1112 *Figure 5. Lapse rates of (a) total annual precipitation in the Koshi Basin for the last 10*  
 1113 *years (2003-2012) and (b) mean annual air temperature. The daily missing data*  
 1114 *threshold is set to 10%. Only stations presenting at least 5 years of data (black points)*  
 1115 *are considered to create the regressions (the bars represent two standard deviations).*  
 1116 *Gray points indicate the stations presenting less than 5 years of data.*

1117



1118

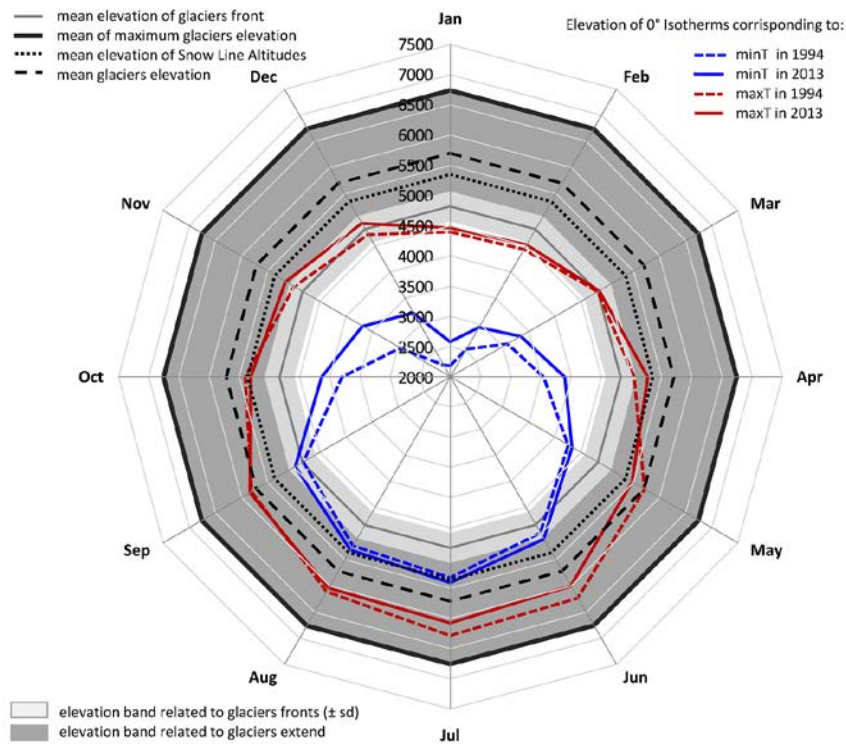
1119 *Figure 6. Spatial distribution of the Sen's slopes in the Koshi Basin for minimum (a),*  
 1120 *maximum (b), and mean (c) air temperature and (d) total precipitation for the 1994-*  
 1121 *2013 period. Data are reported in Table 2.*



1122

1123 *Figure 7. Elevation dependency of minimum (a), maximum (b), and mean (c) air*  
 1124 *temperatures with the Sen's slopes for the 1994-2013 period. The circle indicates*  
 1125 *stations with less than 10% of missing daily data, and the star indicates stations*  
 1126 *showing a trend with  $p$ -value  $< 0.1$ . The red marker represents the trend and the*  
 1127 *associated uncertainty (two standard deviations) referred to the reconstructed time*  
 1128 *series for the AWS1 station (Pyramid). Data are reported in Table 2.*

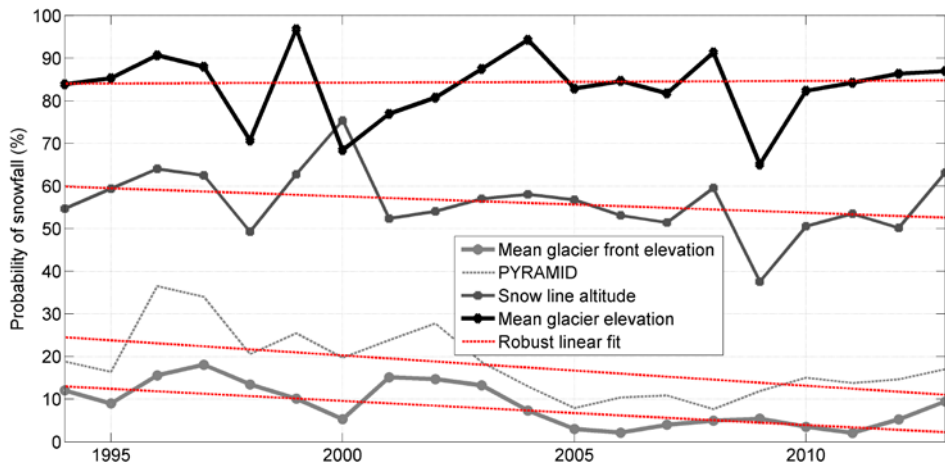
1129



1130

1131 *Figure 8. Linkage between the temperature increases and altitudinal glacier*  
 1132 *distribution. The 0 °C isotherms corresponding to the mean monthly minimum and*  
 1133 *maximum temperature are plotted for the 1994 and 2013 years according the observed*  
 1134 *T trends and lapse rates.*

1135



1136

1137 *Figure 9. Trend analysis of annual probability of snowfall on total cumulated*  
 1138 *precipitation. The red lines represents the robust linear fitting of the time series*  
 1139 *characterized by the associated Sen's slope (more details in the caption of Fig. 3).*